

A 2D Process-Based Model for Suspended Sediment Dynamics: a first Step towards Ecological Modeling

F. M., Achete¹; M. van der Wegen¹; D. Roelvink^{1,2,3} and B. Jaffe⁴

[1]{UNESCO-IHE, Delft, The Netherlands}

[2]{Deltares, Delft, The Netherlands}

[3]{Delft University of Technology, Delft, The Netherlands}

[4]{US Geological Survey Pacific Science Center, Santa Cruz, California}

Correspondence to: F. M. Achete (f.achete@unesco-ihe.org)

Abstract

In estuaries Suspended Sediment Concentration (SSC) is one of the most important contributors to turbidity, which influences habitat conditions and ecological functions of the system. Sediment dynamics differ depending on sediment supply and hydrodynamic forcing conditions that vary over space and over time. A robust sediment transport model is the first step towards a chain of models enabling simulations on contaminants, phytoplankton and habitat conditions.

This work aims to determine turbidity levels in the complex-geometry Delta of San Francisco Estuary using a process-based approach (Delft3D Flexible Mesh software). Our approach includes a detailed calibration against measured SSC levels, a sensitivity analysis on model parameters, and the determination of a yearly sediment budget as well as an assessment of model results in terms of turbidity levels for a single year (Water Year 2011).

Model results show that our process-based approach is a valuable tool in assessing sediment dynamics and their related ecological parameters over a range of spatial and temporal scales and which may act as the base model for a chain of ecological models assessing the impact of climate change and management scenarios. Here we present a modelling approach with limited data producing reliable predictions, which is useful findings for less monitored estuaries.

1 Introduction

Rivers transport water and sediments to estuaries and oceans. Sediment dynamics will differ depending on sediment supply and hydrodynamic forcing conditions varying over space and over time. Many river basins are subjected to slow morphodynamic adaptation due to (gradually) changing forcing conditions, ranging from sea level rise and climate change to anthropogenic developments such as reservoir construction in the watershed.

The human impact on sediment production dates from 3000 years ago, and has been accelerating over the past 1000 years due to considerable engineering works (Syvitski and Kettner, (2011). Milliman and Syvitski (1992) estimate that the budget of sediment delivered to the coastal zone varies between 9.3 and 58 Gt per year. Estimating the world sediment budget is still a challenge either due to lack of data or detailed model studies in this field (Vörösmarty et al., 2003). Adding to that, there is considerable uncertainty in hydraulic forcing conditions and sediment supply dynamics due to variable adaptation timescales over seasons and years (such as varying precipitation and river flow), decades (such as engineering works) and centuries to millennia (sea level rise and climate change).

Examples of anthropogenic changes in sediment dynamics in river basins and estuaries are manifold, e.g. San Francisco Bay-Delta (Schoellhamer, 2011), Yangtze Estuaries (Yahg, 1998) and Mekong Delta (Manh et al., 2014). These three systems present similar conditions of anthropogenic forced sediment supply. After an increase in sediment supply (due to hydraulic mining and deforestation respectively) each had a steep drop in sediment discharge (30%) due to reservoir building and further estuarine clearance after depletion of available sediment in the bed. This implies a) continuous change in sediment dynamics and hence sediment budget in the estuary; b) change in sediment availability leading to change in turbidity levels.

Turbidity is a measurement of light attenuation in water and it is a key ecological parameter. Fine sediment is the main contributor to turbidity. Therefore suspended sediment concentration (SSC) can be translated into turbidity applying empirical formulations. Besides SSC, algae, plankton, microbes and other substances may also contribute to turbidity levels (ASTM International, 2002). High turbidity levels limit photosynthesis activity by phytoplankton and microalgae, therefore decreasing associated primary production (Cole et al., 1986). Turbidity levels also define habitat conditions for endemic species (Davidson-Arnott et al., 2002). We can cite the Delta Smelt as an example seeking for regions where the

turbidity is between 12-18NTU to hide from predators (Bakersville-Bridges, 2004;Brown et al., 2013). Examples of other ecological impacts related to SSC are for vegetation stabilization (Morris et al., 2002;Whitcraft and Levin, 2007), and salt marsh survival under sea level rise scenarios (Kirwan et al., 2010;Reed, 2002).

To assess the aforementioned issues, the goal of this work is to provide a detailed analysis of sediment dynamics concerning a) SSC levels, in the Sacramento-San Joaquin Delta (Delta) area, b) sediment budget and c) translate theses results in turbidity levels, by means of a two dimensions in the horizontal, averaged in the vertical dimension (2DH), process-based, numerical model. The 2DH model solves the 2D vertical integrated shallow water equations coupled with advective-diffusive transport. This process-based model will be able to quantify high resolution sediment budgets and SSC, both in time (~ monthly/yearly) and space (~10s-100s of m). We selected the Delta area as a case study, since the area has been well monitored so that detailed model validation can take place, it hosts endemic species, and allow us to use a 2DH model approach.

The Delta and Bay are covered by a large survey network, offering freely available data on river stage, discharge and suspended sediment concentration (SSC) amongst other parameters, and maintained by USGS (nwis.waterdata.usgs.gov), by Californian Department of Water Resources (<http://cdec.water.ca.gov/>) and National Oceanic and Atmospheric Administration (<http://tidesandcurrents.noaa.gov/>). The continuous SSC measurement stations are periodically calibrated by water collection in situ, filtered and weighted in the laboratory. On top of that, the Bay-Delta system has a high resolution bathymetry available (10m) for all the channels and bays (<http://www.d3d-baydelta.org/>).

Regarding ecological value, starting from the bottom of the food web, the Delta is the most important area for primary production in the San Francisco Estuary. The Delta is one order of magnitude more productive than the rest of the estuary (Jassby et al., 2002;Kimmerer, 2004). It is an area for spawning, breeding and feeding for many endemic species of fishes and invertebrates, including some endangered species like delta smelt (Brown et al., 2013), Chinook salmon, spring run salmon and steelhead. Additionally, Several projects for marsh restoration in the Delta are planned and the success of these projects depends on sediment availability (Brown, 2003).

SSC spatial distribution and temporal variability is important information for the ecology of estuaries. However, observations including both high spatial and temporal resolution of SSC

are difficult to make, so we revert to a coupled hydrodynamic-sediment transport models to make predictions at any place and time and conduct scenario analyses with them.

For the first time, a detailed, process-based model is developed for San Francisco Bay-Delta, to focus on the complex Delta sediment dynamics (MacWilliams et al., 2015). From this model it is possible to describe the spatial sediment (turbidity) distribution and deposition patterns that are important indicators to assess habitat conditions. Analyzing seasonal and yearly variations in sediment dynamics and translating these into turbidity levels to be used as indicators for ecological modeling (Janauer, 2000), this work fills gap the between the physical aspects (hydrodynamic and sediment modeling) and ecology modeling. Previous work focused on understanding the San Francisco Bay-Delta system through data analysis (Barnard et al., 2013;Manning and Schoellhamer, 2013;McKee et al., 2006;McKee et al., 2013;Morgan-King and Schoellhamer, 2013;Schoellhamer, 2011;Schoellhamer, 2002;Wright and Schoellhamer, 2004, 2005), while similar work in other estuaries around the world does not give the direct link to ecology (Manh et al., 2014).

2 Study area and Model

San Francisco Estuary is the largest estuary on the U.S. West Coast. The estuary comprises San Francisco Bay and the inland Sacramento-San Joaquin Delta (Bay-Delta system), which together cover a total area of 1235 km² with a mean water depth of 4.6 meter (Jassby et al., 1993). The system has a complex geometry consisting of interconnected sub-embayments, channels, rivers, intertidal flats, and marshes (**Fig 1**). The Sacramento-San Joaquin Delta (Delta) is a collection of natural and man-made channel networks and leveed islands, where the Sacramento River and the San-Joaquin River are the main tributaries followed by Mokelumne River (Delta Atlas, 1995). San Francisco Bay has 4 sub-embayments. The most landward is Suisun Bay followed by San Pablo Bay, Central Bay (connecting with the sea through Golden Gate) and, further southward, South Bay.

Tides propagate from Golden Gate into the Bay and most of the Delta up to Sacramento (FPT) and Vernalis (VNS) when river discharge is low. Suisun Bay experiences mixed diurnal and semidiurnal tide that ranges from about 0.6 m during the weakest neap tides to 1.8 m during the strongest spring tides. During high river discharge the 2psu isohaline is located in San Pablo bay while during low river discharge it can go landwards of Chipps Island (westernmost reach of the black rectangle, **Fig 1**). The topography highly influences the wind

1 climate in the Bay-Delta system. Wind velocities are strongest during spring and summer
2 presenting afternoon north-westerly gusts of about 9 ms^{-1} (Hayes et al., 1984).

3 San Francisco estuary collects 40% of the total Californian fresh water discharge. It has a
4 Mediterranean climate, with 70% of rainfall concentrated between October and April (winter)
5 decreasing until the driest month September (summer) (Conomos et al., 1985). The
6 orographic lift of the Pacific moist air linked to the winter storms and the snowmelts in early
7 spring govern this wet (winter) and dry (summer) season variability. This system leads to a
8 local hydrological 'Water Year' (WY) definition from 1st October to 30th September, including
9 a full wet season in one WY.

10 It is important to notice that Sacramento and San Joaquin Rivers, together, account for 90% of
11 the total fresh water discharge to the estuary (Kimmerer, 2004). The daily inflow to the Delta
12 follows the rain and snowmelt seasonality, with average dry summers with discharges of 50-
13 $150 \text{ m}^3\text{s}^{-1}$ and wet spring/winter reaching peak discharges of $800\text{-}2500 \text{ m}^3\text{s}^{-1}$. The geographic
14 and seasonal flow concentration leads to several water issues related to agricultural use,
15 habitat maintenance and water export. On a yearly average $300\text{m}^3\text{s}^{-1}$ of water is pumped from
16 South Delta to southern California. The pumping rate is designed to keep the 2psu (salinity)
17 line landwards of Chipps Island avoiding salinity intrusion in the Delta. Allowing the 2DH
18 modeling approach.

19 The hydrological cycle in the Bay-Delta determines the sediment input to the system, thus
20 biota behavior. McKee (2006) and Ganju and Schoellhamer (2006) observed that a large
21 volume of sediment passes through the Delta and arrives to the Bay in a yearly pulse. They
22 estimated that in 1 day approximately 10% of the total sediment volume could be delivered
23 and in extremely wet years up to 40% of the total sediment volume can be delivered in 7 days.
24 During wet months more than 90% of the total sediment inflow is supplied to the Delta.

25 The recent Delta history is dominated by anthropogenic impacts. In the 1850`s hydraulic
26 mining started after placer mining in rivers became unproductive. Hydraulic mining
27 remobilized a huge amount of sediment upstream of Sacramento. By the end of the nineteenth
28 century the hydraulic mining was outlawed leaving approximately $1.1 \times 10^9 \text{ m}^3$ of remobilized
29 sediment, which filled mud flats and marshes up to 1 meter in the Delta and Bay (Wright and
30 Schoellhamer, 2004; Jaffe et al., 2007b). At the same time of the mining prohibition, civil
31 works such as dredging and construction of levees and dams started, reducing the sediment
32 supply to the Delta (Delta Atlas, 1995; Whipple et al., 2012).

1 Typical SSC in the Delta ranges from 10 to 50 mg L⁻¹, except during high river discharge
2 when SSC can exceed 200 mg L⁻¹ reaching values over 1000mgL⁻¹ (McKee et al.,
3 2006;Wright and Schoellhamer, 2005). A sediment budget reflects the balance between
4 storage, inflow and outflow of sediment in a system. Studies based on sediment inflow and
5 outflow, estimated that about two-third of the sediment entering the system deposits in the de
6 Delta (Schoellhamer et al., 2012;Wright and Schoellhamer, 2005). The remaining third is
7 exported to the Bay, and represents on average 50% of the total Bay sediment supply (McKee
8 et al., 2006), the other half comes from smaller watershed around the Bay (McKee et al.,
9 2013).

10 Several studies have been carried out to determine sediment pathways and to estimate
11 sediment budgets in the Delta area (Schoellhamer et al., 2012;Jaffe et al., 2007a;Gilbert,
12 1917;McKee et al., 2013;McKee et al., 2006;Wright and Schoellhamer, 2005). These studies
13 were based on data analysis and conceptual hindcast models. Although the region has a
14 unique network of surveying stations, there are many channels without measuring stations.
15 This might lead to incomplete system understanding and knowledge deficits for the
16 development of water and ecosystem management plans. The monitoring stations are located
17 in discrete points hampering spatial analysis. Also, the impact of future scenarios related to
18 climate change (i.e. sea level rise and changing hydrographs) or different pumping strategies
19 remains uncertain.

20 **2.1 Model description**

21 Structured grid models such as Delft3D and ROMS (Regional Oceanic Modeling System)
22 have been widely used and accepted in estuarine hydrodynamics and morphodynamics
23 modeling including San Francisco Estuary (Ganju and Schoellhamer, 2009;Ganju et al.,
24 2009;van der Wegen et al., 2011). In all these cases the Delta was schematized as 2 long
25 channels since the grid is not flexible to have a 2D modeling of the rivers, channels and
26 flooded island of the system together with the Bay.

27 In case of complex geometry unstructured grids or finite volume model is more suitable.
28 There are three widely known unstructured grid models the TELEMAC-MASCARET
29 (Hervouet, 2007), the UnTRIM (Casulli and Walters, 2000;Bever and MacWilliams, 2013)
30 and D3D FM (Kernkamp et al., 2010). The two first models are purely triangle based and are
31 not coupled (yet) with sediment transport and/or water quality and ecology model.

The numerical model applied in this work is Delft3D Flexible Mesh (D3D FM). D3D FM allows straightforward coupling of its hydrodynamic modules with water quality model, Delft-WAQ (DELWAQ), which gives flexibility to couple with the habitat (ecological) model. D3D FM is a process-based unstructured grid model developed by Deltares (Deltares, 2014). It is a package for hydro- and morphodynamic simulation based on a finite volume approach solving shallow-water equations applying a Gaussian solver. The grid can be defined in terms of triangles, (curvilinear) quadrilaterals, pentagons and hexagons, or any combination of these shapes. It is important to note that (orthogonal) quadrilaterals are the most computationally efficient cells. Kernkamp (2010) and the D3D FM manual (Deltares, 2014) describe in detail the grid aspects and the numerical solvers.

The Bay area and river channels are defined by consecutive curvilinear grids (quadrilateral). Different resolution grid, the river discharging in the Bay, and channel junctions are connected by triangles (**Fig 2**). The average cell size ranges from 1200m x 1200m, in the coastal area, to 450x600m in the Bay area down to 25x25m in the Delta channels. In the Delta, each channel is represented by at least 3 cells in the across-channel direction (**Fig 2**). The grid flexibility allows including the entire Bay-Delta in a single grid containing 63.844 cells from which about 80% are rectangles keeping the computer run times at an acceptable level. It takes 6 real days to run 1 year of hydrodynamics simulation and 12 hours to run the sediment module on an 8 cores desktop computer. Not counting the triangular grid orthogonality issues, in the case of entirely triangular grid the running time for a 1 year simulation would increase from ~72 clock hours to ~192 hours.

We assume that the main flow dynamics in the Delta are 2D meaning no vertical stratification. The Delta does not experience salt-fresh water interactions due to the pumping operations and we assume that temperature differences do not govern flow characteristics. D3D FM generates hydrodynamic output for off-line coupling with water quality model DELWAQ (Deltares, 2004). Off-line coupling enables faster calibration and sensitivity analysis. DFlow-FM generates time series of the following variables: cell link area; boundary definition; water flow through cell link; pointer file gives information concerning neighbors' cells; cell surface; cell volume; and shear stress file, which is parameterized in DFlow-FM using Manning's n . Given a network of water levels and flow velocities (varying over time) DELWAQ can solve the advection-diffusion-reaction equation for a wide range of substances including fine sediment, the focus of this study. DELWAQ solves sediment source and sink

terms by applying the Krone-Parteniades formulation for cohesive sediment transport (Krone, 1962; Ariathurai and Arulanandan, 1978) (Eq.1, Eq.2).

$$D = w_s * c * (1 - \tau_b / \tau_d) \quad (1)$$

$$E = M * (\tau_b / \tau_e - 1) \quad \text{for } \tau_b > \tau_e \quad (2)$$

Where; D Deposition flux of suspended matter ($\text{mg m}^{-2}\text{s}^{-1}$), w_s settling velocity of suspended matter (ms^{-1}), c concentration of suspended matter near the bed (mg m^{-3}), τ_b bottom shear stress (Pa) τ_d critical shear stress for deposition (Pa), E erosion rate ($\text{mg m}^{-2}\text{s}^{-1}$), M first order erosion rate ($\text{mg m}^{-2}\text{s}^{-1}$), τ_e critical shear stress for erosion (Pa).

Note: Following Winterwerp ({Winterwerp, 2006 #402}) we assume that deposition takes place regardless of the prevailing bed shear stress. τ_d is thus considered much larger than τ_b and the second term in equation (Eq. 1) is close to zero.

2.2 Initial and Boundary Conditions

The Bay-Delta is a well measured system; therefore all the input data to the model are in situ data. Initial bathymetry has 10m grid resolution, which is based on an earlier grid (Foxgrover et al., <http://sfbay.wr.usgs.gov/sediment/delta/>), modified to include new data by Wang and Ateljevich

(<http://baydeltaoffice.water.ca.gov/modeling/deltamodeling/modelingdata/DEM.cfm>) and further refined. The bathymetry is based on different data sources including bathymetric soundings and LiDAR data. The hydrodynamic model includes real wind, which results from the model described by (Ludwig and Sinton, 2000). The wind model interpolates hourly data from more than 30 meteorological stations into regular 1km grid cells. Levees and temporal barriers are included in the model considering their deployment time (http://baydeltaoffice.water.ca.gov/sdb/tbp/web_pg/tempbsch.cfm).

The hydrodynamic model has been calibrated for the entire Bay-Delta system (see appendix A and <http://www.d3d-baydelta.org/>). Initial SSC was set at 0mgL^{-1} over the entire domain because the model is initiated during dry period when SSC is low and the initial condition rapidly dissipates. The initial bottom sediment availability defined available mud at places shallower than 5 meters below Mean Sea Level (MSL) including intertidal mud flats, and sand at places deeper than 5 meter below MSL, which are primarily channel regions. This implies that the main Delta channels such as, Sacramento, San Joaquin, Mokelumne are

defined as sandy with few mud patches. The smaller channels and the flooded islands such as Franks Tract are initialized with a muddy bottom. DELWAQ does not compute morphological changes or bed load transport.

In this study we applied 5 open boundaries. Seaward we set hourly water level time series derived from Point Reyes station (tidesandcurrents.noaa.gov/). The other four landward boundaries are river discharge boundaries at Sacramento River (Freeport), Yolo Bypass (upstream water divergence from Sacramento River), San Joaquin River and Mokelumne River. Studies show that Sacramento River accounts for 85% of the total sediment inflow to the Delta, while San Joaquin accounts for 13% (Wright and Schoellhamer, 2005), so it is reasonable to apply 2 sediment discharge boundaries at Sacramento and San Joaquin River. All river boundaries present unidirectional flow, excluding tidal influence.

The river water flow hourly input data are from the following stations, at Sacramento River at Freeport (FPT), San Joaquin River near Vernalis (VNS) and Yolo Bypass (YOLO) were obtained from California Data Exchange Center website (cdec.water.ca.gov/) (Fig 23). The sediment input data, for both input stations FPT and VNS, and calibration stations S Mokelumne R (SMR), N Mokelumne R (NMR), Rio Vista (RVB), Mokelumne (MOK), Little Potato Slough (LPS), Middle River (MDM), Stockton (STK), Mallard Island (MAL) (Fig 2), was obtained by personal communication from USGS Sacramento; this data is part of a monitoring program (<http://sfbay.wr.usgs.gov>). Since 1998, USGS has continuous measuring stations for sediment concentration which is derived from backscatter sensors (OBS) measurements every 15 minutes, and nearly monthly calibrated with bottle samples (Wright and Schoellhamer, 2005).

The SSC data that is used to compare to model results are derived from optical backscatter sensors (OBS). This type of sensor converts scattered light from the particles in photocurrent, which is proportional to SSC. To define the rating curve it is necessary to sample water, filter and weight the filter. However, in some locations the cloud of points when correlating photocurrent and filtered weight shows a large scatter. Large scatter leads to errors in translating photocurrent to SSC. These errors are due to (amongst others) particle size, desegregation (cohesiveness, flocculation, organic-rich estuarine mud); shape effects; sediment-concentration effect (Kineke and Sternberg, 1992; Downing, 2006; Sutherland et al., 2000; Gibbs and Wolanski, 1992; Ludwig and Hanes, 1990). Wright and Schoellhamer (2005)

showed that for the Sacramento-San Joaquin Delta these errors can sum up to 39%, when calculating sediment fluxes through Rio Vista.

In this work we modeled the 2011 water year - 1st October 2010 until 30th September 2011. First, we ran D3D FM for this year to calculate water level, velocities, cell volume and shear stresses. Then, the 1 year hydrodynamic results were imported in DELWAQ which calculated SSC levels.

The SSC model results are compared to in situ measured SSC data. The calibration process assesses the sensitivity of sediment characteristics such as fall velocity (w_s), critical shear stress (τ_{cr}) and erosion coefficient (M). The model outputs are the spatial and temporal distribution of SSC (turbidity), yearly sediment budget for different Delta regions, and the sediment export to the bay.

3 Results

Our focus is to represent realistic SSC levels capturing the peaks, timing and duration, and to develop a sediment budget to assess sediment trapping in the Sacramento-San Joaquin Delta, (Fig 1, highlighted by the black rectangle). Throughout the following sections the results are analyzed in terms of tide averaged results, meaning that the data and model results are filtered to frequencies lower than 2 days. We applied a Butterworth filter with cut off frequency of $1/30\text{h}^{-1}$ as presented in Ganju and Schoellhamer (2006).

3.1 Calibration

The results shown below are derived from an extensive calibration process where the different sediment fractions parameters (w_s , τ_{cr} and M) were tested. The first attempt applied multiple fraction settings presented in previous works (van der Wegen et al., 2011; Ganju and Schoellhamer, 2009). However, tests with a single mud fraction proved to be consistent with the data, representative of the sediment budget, and allow a simpler model setting and better understanding of the SSC dynamics. In addition, with a single fraction it was possible to reproduce more than 90% of the sediment budget for the Delta compared with data calculated sediment budget.

The best fit of the calibration process ($u\text{RMS}=1$ and $\text{skill}=0.8$) for the entire domain defines the standard run. It has w_s of 0.25mms^{-1} , τ_{cr} erosion of 0.25Pa and M of $10^{-4}\text{kgm}^{-2}\text{s}^{-1}$. The

initial bed sediment availability is defined by 1 mud (shoals) and 1 sand (channels) fraction. The analysis present below is based in the standard run, and the sensitivity analysis varies the 3 parameters using the standard run as mid-point.

3.2 Suspended Sediment Dynamics (water year 2011)

The 2011 WY simulation reproduces the SSC seasonal variation in the main Delta regions such as the North (Sacramento River) represented by Rio Vista station (RVB); the South (San Joaquin River) represented by Stockton (STK); Central-East Delta represented by Mokelumne station (MOK) and Delta output represented by Mallard Island (MAL) (Fig 4).

All stations clearly reproduce SSC peaks during high river flow periods during November to July and lower concentrations during the remainder of the year (apart from MAL during the July-August period). The good representation of the peak timing indicates that the main Delta discharge event is reproduced by the model as well as the periods of Delta clearance. These two periods are critical for ecological models, and a good representation generates robust input to ecological models. The differences found between the model and data are further discussed in appendix B.

3.3 Sensitivity analysis

3.3.1 Sediment fraction analysis

We considered one fraction for simplicity and because it reproduces more than 90% of the sediment budget throughout the Delta as well as the seasonal variability of SSC levels. Although more mud fractions considerably increase running time, several tests with multiple fractions were done to explore possibilities for improving the model results.

Including heavier fractions changes the peaks timing and also lowers the SSC curve. Comparing the standard run ($ws=0.25\text{mm s}^{-1}$, $T=0.5\text{Pa}$, $M=10^{-4}\text{ kg m}^{-2}\text{s}$ and bottom composition with mud available shallower than 5 meters) to another run considering 15% of heavier fraction ($ws=1.5\text{mm s}^{-1}$) and 30% of a lighter fraction ($ws=0.15\text{mm s}^{-1}$), showed that the peak magnitudes were underestimated but the first peak timing is closer to the data and the spurious peak mid May is lower.

To be able to find a single best parameter setting a sensitivity analysis was done varying the main parameters in the Krone-Parteniades formulation (Table 1). Regarding sediment flux,

these tests show that some stations, such as RVB and MAL, are more sensitive to parameter change than others, such as STK (**Fig 5**). The model results are most sensitive to the critical shear stress for erosion (T) and least sensitive to the erosion coefficient (M). Analyzing the time series, one concludes that in stations where the fluxes are higher, the change in critical shear stress is less important, since during most of the time the shear stress is already higher than any given critical shear stress.

We are analyzing two metrics, the unbiased Root Mean Square Error (uRMSe, Fig 6) and Skill (Skill, Fig 6) (Bever and MacWilliams, 2013). The uRMSe analyzes the variability of the model relative to the data, in this case 0 is the case when the model and data have equal variability, positive values indicate more model variability and negative values indicate less model variability.

$$uRMSe = \left(\frac{1}{N} \sum_{i=1}^N [(X_{mi} - \overline{X_m})(X_{oi} - \overline{X_o})]^2 \right)^{0.5} \quad (3)$$

Where N is the time series size, X is the variable to be compared, in this case SSC, and \overline{X} is the time-averaged value. Subscript m and O represent modeled and observed values, respectively.

Skill is a single quantitative metric for model performance (Willmott, 1981). When skill equals 1 the model perfectly reproduces the data. The 2 metrics were evaluated at RVB, STK and MAL, representing respectively Sacramento River, San Joaquin River and Delta output.

$$Skill = 1 - \left[\sum_{i=1}^N |X_{mi} - \overline{X_{oi}}|^2 \right] / \left[\sum_{i=1}^N (|X_{mi} - \overline{X_o}| + |X_{oi} - \overline{X_o}|)^2 \right] \quad (4)$$

One notices that changing a parameter can lead to better results in one station but worse in other stations (Fig 6). The choice of the standard run analyzed throughout the paper comes from this analysis as well as the budget analysis. We note that both uRMSe and Skill varies up to 50% over the different runs.

3.4 Initial bottom composition

To study the importance of initial bottom sediment availability we considered 2 cases; one excluding sediment (no sediment available at the bed) and the other by defining available mud at places shallower than 5 meters below Mean Sea Level (BMSL) including intertidal mud

flats and sand at places deeper than 5 meter below MSL being mainly channel regions (the same setting as the standard run).

We did some test varying the 5m threshold. From 3 to 10 meters the final results are all similar. However, considering mud availability in the channels deeper than 10 meters starts to disturb the SSC levels. Time series of SSC comparing the 2 cases and data show that bottom composition has virtually no influence on SCC after the first couple of days. This result also applies for different mud fractions availability and opens horizons for modeling less measured estuaries where virtually no bottom sediment data is available.

Another test shows that it is better to initialize the model with a no sediment at bed than with mud available in the entire domain. Initializing the channels with loose mud generates unrealistically high SSC levels through the years, which can take up to 5 years to be reworked.

4 Discussion

In the previous section we presented the model calibration, a normal practice in the modeling process. In this section we discuss the new insights that were derived from the model results. Although these insights are specific to the San Francisco Bay-Delta system, the same approach can be applied to other estuaries and deltas. The model shows detailed sediment dynamics and the main paths that sediment is transported in the Delta. Sediment flux calculations define the sediment dynamics while gradients in sediment describe the sediment distribution and deposition pattern in the Delta. We also discuss daily and seasonal variation of turbidity levels.

4.1 Spatial sediment distribution

Starting the analysis with the general Delta behavior, during dry periods SSC in the entire Delta is low ($<20\text{mgL}^{-1}$) and the Delta water is relatively clear. The current model results confirm and compile data showing that the Sacramento River is the main sediment supplier into the Delta (Wright and Schoellhamer, 2004; Schoellhamer et al., 2012). Sacramento River peak flow fills the north and partially fills the central/east Delta with sediment. However, the rest of the Delta keeps quite low levels ($\sim 20\text{mgL}^{-1}$) of SSC all year long. Passing Vernalis (VNS), San Joaquin River main branch flows to the east, however the SSC peak reaches no much further than STK. The west branch goes toward the water pumping stations where to the

sediment is pumped out of the system. This behavior reflects in very low SSC in the South Delta (Old River and Franks Tract) region, which are deposition areas.

Three Mile Slough (TMS) and the Delta Cross Channel (DCC) connect the Sacramento River with the central and eastern Delta. Model results show that together they carry 60Kton per year of sediment southward. DCC operation defines SSC levels in the eastern/central Delta to a large extent. To show the importance of DCC we run the model twice, one with DCC always open and one always closed. When DCC is open, high SSC Sacramento river water (~150mgL⁻¹) flows towards Mokelumne River and Eastern Delta increasing the overall SSC in the area. When it is closed SSC levels in central and eastern delta are about 30mgL⁻¹ lower than in the previous case (Fig 7). The effect of opening DCC can be observed in the SSC level at the San Joaquin River from MOK station seawards. In the Sacramento River, the opening decreases SSC levels, by about 10mgL⁻¹. It affects the river SSC all the way to Mallard Island (Fig 7).

During peak river discharge, Sacramento River sediment reaches Mallard Island in approximately 3 days, Carquinez Straight in 5 days, and the Golden Gate Bridge in approximately 10 days. This timing is proportional to river discharge. However from Mallard Island seawards it is a rough estimate due to the 2D approximation. The San Joaquin River sediment remains largely trapped in the southern Delta. The flooded islands, breached levees like Franks Tract, present a different behavior. During the entire year the SSC levels are below 15mg L⁻¹, the river peak discharge signal does not affect them.

Sediment flux is a useful tool for a quantitative and qualitative analysis of the sediment path and its derivative gives sedimentation/erosion patterns. It is defined by the product of water velocity (U), times Cross-sectional area (A) times SSC (C) (Eq. 5).

$$F_{sed} = U * A * C \quad (5)$$

The yearly sediment flux through FPT from model results is 1132Kt yr⁻¹ (thousand metric tons per year) against 1096Kt yr⁻¹ from data, following Sacramento River we have RVB with 832Kt yr⁻¹ (994Kt yr⁻¹, data), then MAL with 617Kt yr⁻¹ (654 Kt yr⁻¹) (Fig 8). We calculate that 30Kt yr⁻¹ of Sacramento River sediment flows to the eastern Delta through DCC, 30 Kt/yr through TMS and 20Kt yr⁻¹ from Georgina Slough. San Joaquin River carries 490Kt yr⁻¹ (498) through VNS, heading to STK with 205Kt yr⁻¹ (190Kt yr⁻¹). It was estimated that 100Kt

1 yr^{-1} was exported through pumping. To close the system in central Delta, the flux through JPT
2 is 126Kt yr^{-1} (no data) and DCH approximately 0 (no data) (Fig 8).

3 Seaward from MAL considerable salt-freshwater stratification takes place in the water column
4 These 3D effects are not captured by our 2DH approach so that the model results in this
5 region are disregarded. Therefore, Fig 8 shows preliminary sediment flux to the Bay by a
6 dashed line.

7 **4.2 Sediment budget**

8 From the previous section one can see that more sediment enters ($\sim 1600\text{ Kt yr}^{-1}$) than leaves
9 ($\sim 600\text{ Kt yr}^{-1}$) the Delta. So by mass conservation law, the difference between inflow and
10 outflow deposits in the Delta. Jaffe et al.(2007b) developed a box model based on bathymetry
11 data to define sediment budget of the Delta and Bay to define sediment availability for
12 ecology purposes. The model results agree with data estimations that about two third of the
13 sediment input is retained in the Delta (Schoellhamer et al., 2012;Wright and Schoellhamer,
14 2005), and it is consistent throughout the years (Cappiella et al., 1999;Jaffe et al.,
15 1998;Wright and Schoellhamer, 2004). Because of the detailed description of the sediment
16 path, it is possible to further understand and describe the sediment budget in Delta sub-
17 regions (north, central and south), comparing our results to data when available (Morgan
18 King, 2012, personal communication).

19 Besides the overall trend, different parts of the Delta present different trap efficiency. Model
20 results show that Northern Delta (the least efficient) traps $\sim 23\%$; Central/Eastern Delta traps
21 32% , Central/Western 65% , and the most efficient is the Southern Delta region trapping 67%
22 of the sediment input. The highest trapping efficient regions correspond to islands inundated
23 through levee breaching (Wright and Schoellhamer, 2005).

24 From the total Sacramento River sediment input 40% stays in the northern Delta and about
25 40% is exported to Bay area. The remaining 20% deposits in the central/eastern Delta and
26 only 2% travel all the way to South Delta. About 70% of San Joaquin sediment deposits in the
27 southern Delta, 10% go to central Delta, 15% is exported via Clifton Court pumping facilities
28 and 5% is exported to the Bay. This transport is reflected in the bottom composition of the
29 Delta, Sacramento River sediment dominates the Northern and Central Delta and San Joaquin
30 River sediment dominates the Southern Delta bottom composition (Fig 9).

It is possible to divide the sediment budget analysis for the wet and the dry season, since the Delta presents different dynamics for each season. Water year 2011 was a wet year, with the wet season lasting from mid-January until the end of May. During the wet period 60% of the yearly sediment input budget entered the Delta through FPT and VNS and 70% of the yearly budget was exported through MAL. In the wet season the high river water discharges and SSC pulses flushes the entire Delta with sediment. In this season high SSC gradients are observed in the plume fronts leading to rapid changes in habitat conditions for many species. After the front the high SSC level can last for more than a month, indicating changing in habitat conditions

During the dry season the Delta experiences lower river discharges and SSC levels thus the sediment transport is lower as well. In the dry season SSC levels are more uniform not presenting peaks, at this time the water is clear and the advective flux is lower, which is going to be discussed in the next section.

4.3 Sediment flux analysis

SSC peaks at FPT can be tracked down the estuary. At the RVB station the SSC peak follows the same dynamic as observed at FPT; however, this behavior does not apply for the entire Delta. Schoellhamer and Wright (2005) observed that the river signal is attenuated through the estuary. This attenuation can be understood by analyzing changes in the dominant sediment flux component.

Dyer (1974) decomposed the tidally averaged fluxes in three main components: tidal mean, the advective term; tidal fluctuation, the dispersive term; and the Stokes Drift. This decomposition was possible considering that the measured valued is the sum of a tidally mean component $[x]$, and a fluctuating component x' , so $x = [x] + x'$ (Eq.6), substituting in Eq 5 and simplifying the small contribution terms, three main terms remain (Eq.7). The first term of Eq7 is the advective term, it is the river flow as it is calculated by the mean discharge, area and concentration; the second one is the dispersive term that accounts for tidal pumping, which is the compensation flow for the inward transport of the tidal wave the 2 first terms already account for more than 95% of the flux and the Stokes Drift which is the transport due to a variation in the cross-sectional area.

$$[F] = [U][A][C] + [[U'[A]C']] + [[U'A'[C]]] \quad (7)$$

The model allows for a detailed temporal and spatial analysis of the three flux components. The temporal analysis are done in 3 steps, the first one considering the whole year and then splitting in the wet and dry season. For the spatial analysis, we defined 4 stations for each river where the first station is dominated by the river flux and the last experience a mix of tidal and river fluxes. The stations were determined following Sacramento River, starting with FPT, followed by RVB down to Mallard Island the delta output and following San Joaquin River from VNS, to STK and MOK. Three Mile Slough (TMS) and San Joaquin Junction (SJJ) represent the Delta smaller channels.

Sacramento River at FPT, the most landward station, experiences no tidal influence so the flux is purely advective. RVB, seaward, experiences tidal fluctuations and the dispersive flux is responsible for 22% of the total flux; however no Stokes drift flux is present (Fig 10). On the other hand, Stokes Drift component accounts for 33% of the total flux in MAL station implying that tides have a bigger influence in this region.

An analogue can be drawn to San Joaquin branch, where VNS and STK experience only advective terms. In MOK and SJJ dispersive (20% and 63% respectively) and Stokes flux start (5 and 11%) to change the total flux (Fig 10). The analyses of the 3 different flux components in smaller Delta channels show that river and tidal signals are equally important. In other words the river peak signal is less important inside smaller channels than in rivers. At TMS, the dispersive flow accounts for 60% of the total flux.

The fluxes analysis shows that there is no change in the Delta net circulation when comparing wet and dry seasons. In other words, there is not a major signal change in the flux signal direction when comparing the seasons. However, there is a change in importance of each flux component.

Fig 10 shows that dispersive flux and Stokes Drift relative contributions vary seasonally: when river discharge is high the relative contribution of dispersive flux and Stokes Drift is lower than during low flow conditions. This pattern is better observed in stations where the river signal is stronger. At RVB the dispersive flux contribution is about 15% during the wet season and 26% in the dry season, the same applies for MAL and STK. In smaller channels, like TMS and SJJ, The dispersive flux seasonal variation is milder, varying about 10%, from 55% in the wet season and 65% in the dry. In the dry season the change in fluxes contribution, from advective to dispersive and Stokes Drift, leads to a lower net export of sediment from the Delta, even though the concentrations in the Delta about 30mg L^{-1} .

4.4 Sediment deposition pattern

The flux change from completely advective to dispersive and Stokes drift sheds some light on the Delta deposition areas. The places where the dispersive flux starts to play a role, near RVB and MOK areas, are the same places where net deposition is observed (**Fig 11**). Other locations where considerable sedimentation takes place are in flooded islands areas, such as Frank Tract and the Clifton Court. The 2D model allows determining such areas (**Fig 11**).

The San Joaquin River downstream of Stockton experiences high deposition. This finding is confirmed by constant dredging works need to maintain Stockton navigation channel. The river discharge modulates the deposition pattern in the main channels. In the Sacramento River, Rio Vista area (RVB), a rapid deposition takes place just after the peak discharge. Later this deposited sediment is gradually washed away and transported to the mud flats at the channel margins, until the next peak. At flooded island the sedimentation process is gradually and steady, we do not observe erosion in these areas.

Mainly deposition is observed during wet and dry period. Some exceptions occur in small bends in the Sacramento River that goes from eroding (wet season) to depositing areas (dry season). The deposition pattern provides insight into the best areas for marsh restoration.

4.5 Turbidity

So far the discussion was presented in terms of SSC levels, budgets and fluxes, while ecological analysis is often based on turbidity levels. SSC and turbidity are correlated by rating curves as $\log_{10}(\text{SSC}) = a \cdot \log_{10}(\text{Turb}) + b$, where a and b are local parameters empirically defined for each Delta area. The Northern area $a=0.85$ and $b=0.35$; Central/Western area $a=0.91$ and $b=0.29$, Central/Eastern $a=0.72$ and $b=0.26$; Southern $a=1.16$ and $b=0.27$; Eastern $a=0.914$ and $b=0.29$ (USGS Sacramento, personal communication 2014).

In this section we present average values for turbidity within a specific Delta region as well as its seasonal and daily variations (Fig 12). Generally, the mean turbidity levels and spatial variations are higher during the wet season than during the dry season. During the wet season, the Southern area presents the highest mean value (50 ntu), and deviation (15ntu), caused by a combination of large sediment supply and low flow velocities. The Northern region is the second most turbid area (45 ± 10 ntu), where sediment transported by Sacramento River flows in the channels, increasing the turbidity levels. The Central Eastern region is the least turbid

area ($5\pm 2\text{ntu}$) and, as previously shown, it presents the highest trapping efficiency of the entire Delta. In the dry season the mean turbidity daily variation decreases in the whole Delta, excepting the Central/Eastern region. The opening of the DCC during the dry season lets sediment from the Sacramento River entering these areas, increasing the mean turbidity level. The spatial distribution of the most turbid areas is the same as in the wet season. The daily deviation is mostly proportional to the turbidity level and to the distance from the sea. In the Southern and Western areas the daily variation is higher during the dry season. It shows that there is a strong tidal signal in these parts of the Delta.

As for from this work results, we note that the Sacramento to San Joaquin River connecting channels DCC and GLS are important bridges to export sediment from Sacramento to Eastern Delta. On the other hand the smaller channels of the network play a minor role in the Delta sediment budget, since the discharges in these channels are considerably smaller than in the rivers.

4.6 Data input discussion

As a well surveyed area, combining with a complex process-based model, the Delta offers the chance of testing how much data it is necessary to develop a reliable sediment model. The model offers the possibility of having high temporal and spatial resolution, as well as considers multiple physical processes as bottom friction, sedimentation and erosion. The available data allows calibration and validation of model results.

As presented before, with simple settings as 1 mud fraction and simple bed sediment availability the model is capable of representing the main sediment dynamics processes, the peak timing and duration, as well as sediment budget. The necessary data to an accurate modeling and further forecasting is a fine resolution bathymetry to correctly reproduce hydrodynamics, SSC and discharge in the inflow and outflow boundaries. It is necessary as well 1-2 stations in the domain in order to properly calibrate the model. The results from the calibrated model using these few data can be extrapolated for the entire domain, allowing closing the sediment budget for the whole system.

The 2D model results output are available in high temporal (~hours) and spatial (~20 meters) resolution, allowing to translate model results in water quality parameters for modeling or for descriptive purposes. In other words, with limited input data we can come to a detailed system

description with considerable forecast capacity, expanding the applicability of this work to less measured estuaries.

5 Conclusions

In this work we make a step towards the understanding and simulating sediment dynamics from source to sink in a complex estuary. This work shows that it is possible to reproduce the main system sediment dynamics as well as a detailed budget for complex areas such as the Delta using a 2D process based numerical model coupled with a water quality model.

Overall, the model reproduces the SSC peaks and event timing and duration (wet season) as well as the low concentration in dry season throughout the Delta, except at Mallard where water column is stratified due to salt intrusion. Stratification issues are not solved in a 2D model. For this reason we are working on a 3D model in order to include the Bay area, leading to a unique model from source to sink.

The Delta is well covered by observation stations. However, this work shows that the substantial sediment is exported through the pumping stations (100kt yr^{-1}) at the Southern Delta where no data in SSC is available. The sediment exporting needs further investigation, since it is possible that has been deposited in the channels before the pumps.

We show that with simple sediment settings as one fraction at the input boundary and simple distribution of bed sediment availability, it is possible to reproduce seasonal variations as well as define yearly sediment budget with more than 90% of accuracy when compared with data derived budget. It shows also that it is extremely important to have discharge and SSC measurements at least in the input boundaries and close to the system output in order to be able to calibrate the model settings applied for hydrodynamics and suspended sediment. This methodology now can be applied in less measured estuaries.

Sediment is a key-factor to estuaries water quality and ecology. The D3D FM software allows direct coupling to water quality, sediment transport and habitat modeling. Our work provides the basis to a chain of models, which goes from the hydrodynamics, to suspended sediment, to phytoplankton, to fish, clams and marshes. The turbidity and deposition pattern analysis may guide ecologists in future works to define areas of interest and/or vulnerable areas to be study, as well as guide data collecting efforts. The present model opens the possibility for forecast and operational modeling. Forecasting the time frame of high levels of SSC (turbidity) allows planning of measurements campaigns for ecologists, as well as the possibility of tracking

1 potentially contaminated sediment and be able to make a contingency plan as well as
2 temporary barriers and pumping operations.

3 The Sacramento San-Joaquin Delta is a typical case of a highly impacted estuary. Being able
4 to numerically simulate and determine sediment transport, budget and turbidity levels in this
5 type of environment open possibilities to better informed political, ecological and
6 management decisions including how to respond to climate change and sea level rise. This
7 type of model is an important management tool that is applicable to other impacted estuaries
8 worldwide.

9 **Appendix A: Hydrodynamic Calibration**

10 The hydrodynamic calibration was carried out for 3 month high river flow conditions
11 (December 16, 1999 until March 16, 2000) and a 3 month period of low river flow conditions
12 (July 16, 2001 until October 16, 2001). All presented data is with respect to NAVD88
13 (vertical datum), UTM 10 (horizontal datum) and GMT (time reference).

14 Hourly measured water levels at Point Reyes (tidesandcurrents.noaa.gov/) were used as
15 seaward boundary condition. Landward boundary conditions for the Sacramento River were
16 obtained from daily measured river flow data at Freeport (FPT) and for the San Joaquin River
17 near Vernalis (VNS) (cdec.water.ca.gov/). The inflow from the Yolo Bypass was
18 approximated by (Derived after curve fitting data relationship between Qyolo and Qrsac.)

19 Measured data for the Bay area were derived from tidesandcurrents.noaa.gov/, for part of the
20 Delta from the California Data Exchange Centre cdec.water.ca.gov/ and for station with
21 numbers from direct contact with the Department of Water Resources (DWR).

22 Calibration was carried out by systematically varying the value of the Manning's coefficient
23 for different sub-areas of the Bay-Delta system. The calibration data analysis includes (local
24 and time varying) influence of air pressure and wind in the definition of the boundary
25 condition as well as in the calibration data inside the modeling domain. These may account
26 for (part of) the error between measurements and modeling results. Also, the NAVD88
27 reference is not known for all measurement stations, although tidal water fluctuations may be
28 modeled properly. To circumvent these distortions a better method to assess the model
29 performance is to focus on water level amplitude and phasing of the different tidal
30 constituents. Boundary conditions, calibration data and model results are thus decomposed by
31 Fourier transformation into tidal components which are then compared. The following table

gives the results of this analysis for 34 tidal constituents at Golden Gate (GGT) for high river flow conditions. By far, the main tidal constituents at (GGT) are O1, K1, N2, M2 and S2, with M2 being the largest. The model represents their values quite well. The difference in amplitude is 1.3 % for M2, up to 14% for O1, but the phasing shows a maximum of only 3% (O1)).

The Fig A1 gives calibration results for the high and low river flow. The largest (extreme) deviations are explained by the fact that the measured water levels did not have a known reference to NAVD88 (<http://www.d3d-baydelta.org/>).

Appendix B: SSC Calibration

All stations clearly reproduce SSC peaks during high river flow periods and lower concentrations during the remainder of the year (apart from MAL during the July-August period). The good representation of the peak timing means that the main Delta event is reproduced by the model as well as the periods of Delta clearance. These two periods are critical for ecological models, and a good representation generates robust input to ecological models. A closer look at Fig 4 reveals differences between model results and data. Following these differences is discussed station by station in this appendix.

One observes that at RVB, SSC levels are directly proportional to Sacramento River discharge (Fig B3), and that the model properly represents the water discharge peak intensity and duration. However, in the model, the first peak remobilizes sediment faster than observed in the data. Analyzing the raw data, it is possible to observe a trend of SSC increase which the model overestimates. A probable explanation lies on the initial sediment composition of the bed. Defining the bottom sediment composition does not account for consolidation processes; so the first peak comes after the dry season when the mud in the banks has consolidated. In the simulation case, when river discharge increases, it remobilizes non-consolidated bottom/bank sediment causing an earlier peak than in the data; similar behaviour is observed in STK in December. Sediment trapped in subaquatic vegetation and marshes could be another explanation for the slower increase of the first peak as the model discharges for both stations agree with data (Fig 4).

Another difference between the data and the model results in RVB is the peak in May (second rectangle, Fig B1), which is not observed in the data. SSC level at RVB station is directly proportional to water discharge in FPT (Fig B3, RVB). The May peak is observed in FPT and so should have been transported towards RVB just as the two preceding peaks. However, the data set does not reproduce this peak. One of the possible explanations is errors in data measurements, since it comes after a major event and the equipment might be damaged. Other explanations could be a different composition of the suspended sediment properties and/or flocculation.

The model underestimates the first and second SSC peaks at MOK. However, the data SSC signal is not consistent with the local water discharge signal. First, we checked that modeled water discharge is reproducing the local conditions, where data is available from mid-February onwards. The last peak in Fig (mid-March) shows that water discharge, in situ and modeled SSC have the same range of variation. Therefore the SSC levels are proportional to the local water discharge. Backwards in time, the January SSC data peak is much higher than the water discharge and the SSC level calculated in the model. The same happens in mid-February when no water discharge peak is observed but there is a peak in the SSC data. Again the peaks in SSC could be derived from an error in the measurements or local, diffuse input of sediment such as from local farm waste water or biological activity remobilizing the substrate.

The model represents well the wet season SSC peaks at MAL; however, during the three drier periods of the year the model underestimates SSC levels (Fig B2). From the scatter plot water discharge versus SSC (Fig B3**Error! Reference source not found.**), it is possible to explain the weaker performance of the model during low river flow at MAL. These graphs represent river water discharge in FPT lagged by 2 days to SSC in RVB and MAL. Several time lags were tested, as MAL does not present a reasonable correlation with any of the time lags; it is presented here with the same time lag as the one for RVB. RVB station reflects a positive correlation between river discharge and SSC derived from in situ data and model results. The correlation coefficient (R), statistically shows how two variables are correlated, in RVB $R=0.58$.

In MAL station $R=0.26$, showing that there is almost no correlation between river discharge and SSC levels. The low correlation is due to high SSC level in low water discharge periods, when the model underestimates SSC levels. Under low river discharges conditions, salt water intrudes into Suisun Bay leading to considerable stratification between fresh and salt water

1 and shifting of the ETM landward (<http://sfbay.wr.usgs.gov/access/wqdata/>) (Brennan et al.,
2 2002). In order to better model SSC levels at these conditions a 3D model would be needed to
3 reflect conditions at MAL adequately. With this results we are still able to calculate sediment
4 export, since most of the sediment export occurs in the wet period (McKee et al., 2006),
5 when the model reproduces SSC levels.

7 **Acknowledgements**

8 The research is part of the US Geological Survey CASCaDE climate change project
9 (CASCaDE contribution 60). The authors acknowledge the US Geological Survey Priority
10 Ecosystem Studies and CALFED for making this research financially possible. The data used
11 in this work is freely available on the USGS website (nwis.waterdata.usgs.gov). The model
12 applied in this work will be freely available from <http://www.d3d-baydelta.org/>.

References

- Ariathurai, R. and Arulanandan, K.: Erosion rates of cohesive soils, *J. Hydr. Eng. Div.-ASCE*, 104, 279–283, 1978.
- ASTM International: Standards on Disc, Section Eleven, Water and Environmental Technolog, PA, USA, 2002.
- Barnard, P. L., Schoellhamer, D. H., Ja_e, B. E., and McKee, L. J.: Sediment transport in the San Francisco Bay coastal system: an overview, *Mar. Geol.*, 345, 3–17, doi:10.1016/j.margeo.2013.04.005, 2013.
- Beven, K., Smith, P. J., and Wood, A.: On the colour and spin of epistemic error (and what we might do about it), *Hydrol. Earth Syst. Sci.*, 15, 3123–3133, doi:10.5194/hess-15-3123-2011, 2011.
- Bever, A. J. and MacWilliams, M. L.: Simulating sediment transport processes in San Pablo Bay using coupled hydrodynamic, wave, and sediment transport models, *Mar. Geol.*, 345, 235–253, doi:10.1016/j.margeo.2013.06.012, 2013.
- Brennan, M. L., Schoellhamer, D. H., Burau, J. R., and Monismith, S. G.: Tidal asymmetry and variability of bed shear stress and sediment bed flux at a site in San Francisco Bay, USA, *Environmental Fluid Mechanics Laboratory, Dept. Civil& Environmental Engineering, Stanford University, Stanford, CA, US Geological Survey, Placer Hall, Sacramento, CA*, 2002.
- Brown, L., Bennett, W., Wagner, R. W., Morgan-King, T., Knowles, N., Feyrer, F., Schoellhamer, D., Stacey, M., and Dettinger, M.: Implications for future survival of delta smelt from four climate change scenarios for the Sacramento–San Joaquin Delta, California, *Estuar.Coast.*, 36, 754–774, doi:10.1007/s12237-013-9585-4, 2013.
- Brown, L. R.: A Summary of the San Francisco Tidal Wetlands Restoration Series, *San Francisco Estuary and Watershed Science*, 1, 2003.
- Cappiella, K., Malzone, C., Smith, R., and Jaffe, B. E.: Sedimentation and Bathymetry Changes in Suisun Bay: 1867–1990, *USGS, Menlo Park*, 1999.
- Casulli, V., and Walters, R. A.: An unstructured grid, three-dimensional model based on the shallow water equations, *International Journal for Numerical Methods in Fluids*, 32, 331–348, doi:10.1002/(sici)1097-0363(20000215)32:3<331::aid-flid941>3.0.co;2-c, 2000.

1 Cole, B., Cloern, J., and Alpine, A.: Biomass and productivity of three phytoplankton size classes in
2 San Francisco Bay, *Estuaries*, 9, 117–126, doi:10.2307/1351944, 1986.

3 Conomos, T. J., Smith, R. E., and Gartner, J. W.: Environmental setting of San Francisco Bay,
4 *Hydrobiologia*, 129, 1–12, doi:10.1007/BF00048684, 1985.

5 Davidson-Arnott, R. G. D., van Proosdij, D., Ollerhead, J., and Schostak, L.: Hydrodynamics and
6 sedimentation in salt marshes: examples from a macrotidal marsh, Bay of Fundy, *Geomorphology*, 48,
7 209–231, doi:10.1016/S0169-555X(02)00182-4, 2002.

8 Delta Atlas: Sacramento–San Joaquin Delta Atlas, DWR – Department of Water Resources,
9 California, USA, 1995.

10 Deltares: D-Flow Flexible Mesh, Technical Reference Manual, Deltares, Delft, 82 pp., 2014. Downing,
11 J.: Twenty-five years with OBS sensors: the good, the bad, and the ugly, *Cont. Shelf. Res.*, 26, 2299–
12 2318, doi:10.1016/j.csr.2006.07.018, 2006.

13 Dyer, K. R.: The salt balance in stratified estuaries, *Estuar. Coast. Mar. Sci.*, 2, 273–281,
14 doi:10.1016/0302-3524(74)90017-6, 1974.

15 Ganju, N. K. and Schoellhamer, D. H.: Annual sediment flux estimates in a tidal strait using surrogate
16 measurements, *Estuar. Coast. Shelf S.*, 69, 165–178, doi:10.1016/j.ecss.2006.04.008, 2006.

17 Ganju, N. K. and Schoellhamer, D. H.: Calibration of an estuarine sediment transport model to
18 sediment fluxes as an intermediate step for simulation of geomorphic evolution, *Cont. Shelf. Res.*, 29,
19 148–158, doi:10.1016/j.csr.2007.09.005, 2009.

20 Ganju, N. K., Schoellhamer, D. H., and Jaffe, B. E.: Hindcasting of decadal-timescale estuarine
21 bathymetric change with a tidal-timescale model, *Journal of Geophysical Research*, 114,
22 10.1029/2008jf001191, 2009.

23 Gibbs, R. J. and Wolanski, E.: The effect of flocs on optical backscattering measurements of
24 suspended material concentration, *Mar. Geol.*, 107, 289–291, doi:10.1016/0025-3227(92)90078-V,
25 1992.

26 Gilbert, G. K.: Hydraulic-Mining Debris in the Sierra Nevada, Professional Paper 105, USGS,
27 California, USA, 154 pp., 1917.

28 Guo, L., van der Wegen, M., Roelvink, D., and He, Q.: Exploration of the impact of seasonal
29 river discharge variations on long-term estuarine morphodynamic behavior, *Coastal*
30 *Engineering*, 95, 105–116, <http://dx.doi.org/10.1016/j.coastaleng.2014.10.006>, 2015.
31

1 Hayes, T. P., Kinney, J. J., and Wheeler, N. J.: California Surface Wind Climatology, California Air
2 Resources Board, Aerometric Data Division, California, USA, 107 pp., 1984.

3 Hervouet, J.-M.: in: Hydrodynamics of Free Surface Flows, John Wiley & Sons, Ltd, 1-360,
4 2007.

5
6 Jaffe, B. E., Smith, R., and Torresan, L.: Sedimentation and Bathymetric Change in San Pablo Bay:
7 1856–1983, USGS, Menlo Park, 1998.

8 Jaffe, B. E., Smith, R. E., and Foxgrover, A. C.: Anthropogenic influence on sedimentation and
9 intertidal mudflat change in San Pablo Bay, California: 1856–1983, *Estuar. Coast. Shelf S.*, 73, 175–
10 187, doi:10.1016/j.ecss.2007.02.017, 2007.

11 Janauer, G. A.: Ecohydrology: fusing concepts and scales, *Ecol. Eng.*, 16, 9–16, doi:10.1016/S0925-
12 8574(00)00072-0, 2000.

13 Jassby, A. D., Cloern, J. E., and Powell, M. A.: Organic carbon sources and sinks in San Francisco
14 Bay: variability induced by river flow, *Mar. Ecol.-Prog. Ser.*, 95, 39–54, 1993.

15 Jassby, A. D., Cloern, J. E., and Cole, B. E.: Annual primary production: Patterns and
16 mechanisms of change in a nutrient-rich tidal ecosystem, *Limnology and Oceanography*, 47,
17 698-712, 10.4319/lo.2002.47.3.0698, 2002.

18

19 Kernkamp, H. W. J., Van Dam, A., Stelling, G. S., and De Goede, E. D.: Efficient scheme for the
20 shallow water equations on unstructured grids with application to the Continental Shelf, *Ocean*
21 *Dynam.*, 29, 1175–1188, doi:10.1007/s10236-011-0423-6, 2010.

22 Kimmerer, W.: Open water processes of the San Francisco estuary: from physical forcing to biological
23 responses, *San Francisco Estuary and Watershed Science*, 2 pp., 2004.

24 Kineke, G. C. and Sternberg, R.W.: Measurements of high concentration suspended sediments using
25 the optical backscatterance sensor, *Mar. Geol.*, 108, 253–258, doi:10.1016/0025-3227(92)90199-R,
26 1992.

27 Kirwan, M. L., Guntenspergen, G. R., D'Alpaos, A., Morris, J. T., Mudd, S. M., and Temmerman, S.:
28 Limits on the adaptability of coastal marshes to rising sea level, *Geophys. Res. Lett.*, 37, L23401,
29 doi:10.1029/2010gl045489, 2010.

30 Krone, R. B.: Flume Studies of the Transport of Sediment in Estuarial Shoaling Processes, University
31 of California, Berkeley, California, 1962.

- 1 Ludwig, F. L. and Sinton, D.: Evaluating an objective wind analysis technique with a long²⁵ record of
2 routinely collected data, *J. Appl. Meteorol.*, 39, 335–348, doi:10.1175/1520-
3 0450(2000)039<0335:eaowat>2.0.co;2, 2000.
- 4 Ludwig, K. A. and Hanes, D. M.: A laboratory evaluation of optical backscatterance suspended solids
5 sensors exposed to sand-mud mixtures, *Mar. Geol.*, 94, 173–179, doi:10.1016/0025-3227(90)90111-
6 V, 1990.
- 7 Manh, N. V., Dung, N. V., Hung, N. N., Merz, B., and Apel, H.: Large-scale suspended sediment
8 transport and sediment deposition in the Mekong Delta, *Hydrol. Earth Syst. Sci.*, 18, 3033–3053,
9 doi:10.5194/hess-18-3033-2014, 2014.
- 10 Manning, A. J. and Schoellhamer, D. H.: Factors controlling floc settling velocity along a longitudinal
11 estuarine transect, *Mar. Geol.*, 345, 266–280, doi:10.1016/j.margeo.2013.06.018, 2013.
- 12 MacWilliams, M L.; Bever, A J.; Gross, E S.; Ketefian, G S.; & Kimmerer, W J.(2015). Three-Dimensional
13 Modeling of Hydrodynamics and Salinity in the San Francisco Estuary: An Evaluation of Model Accuracy, X2, and
14 the Low-Salinity Zone. *San Francisco Estuary and Watershed Science*, 13(1). jmie_sfews_20703. Retrieved
15 from: <https://escholarship.org/uc/item/7x65r0tf>
16
- 17 McKee, L. J., Ganju, N. K., and Schoellhamer, D. H.: Estimates of suspended sediment entering San
18 Francisco Bay from the Sacramento and San Joaquin Delta, San Francisco Bay, California, *J. Hydrol.*,
19 323, 335–352, doi:10.1016/j.jhydrol.2005.09.006, 2006.
- 20 McKee, L. J., Lewicki, M., Schoellhamer, D. H., and Ganju, N. K.: Comparison of sediment supply to
21 San Francisco Bay from watersheds draining the Bay Area and the Central Valley of California, *Mar.*
22 *Geol.*, 345, 47–62, doi:10.1016/j.margeo.2013.03.003, 2013.
- 23 Milliman, J. D. and Syvitski, J. P. M.: Geomorphic/tectonic control of sediment discharge to the ocean:
24 the importance of small mountainous rivers, *J. Geol.*, 100, 525–544, doi:10.1086/629606, 1992.
- 25 Morgan-King, T. and Schoellhamer, D.: Suspended-sediment flux and retention in a backwater tidal
26 slough complex near the landward boundary of an estuary, *Estuar. Coast.*, 36, 300–318,
27 doi:10.1007/s12237-012-9574-z, 2013.
- 28 Morris, J. T., Sundareshwar, P. V., Nietch, C. T., Kjerfve, B., and Cahoon, D. R.: Responses of coastal
29 wetlands to rising sea level, *Ecology*, 83, 2869–2877,
30 doi:10.1890/00129658(2002)083[2869:rocvtr]2.0.co;2, 2002.
- 31 Reed, D.: Sea-level rise and coastal marsh sustainability: geological and ecological factors in²⁰ the
32 Mississippi delta plain, *Geomorphology*, 48, 233–243, 2002.
- 33 Roelvink, J. A.: Coastal morphodynamic evolution techniques, *Coastal Engineering*, 53, 277-
34 287, 10.1016/j.coastaleng.2005.10.015, 2006.

1

2 Schoellhamer, D. H.: Variability of suspended-sediment concentration at tidal to annual time scales in
3 San Francisco Bay, USA, *Cont. Shelf. Res.*, 22, 1857–1866, doi:10.1016/S0278-4343(02)00042-0,
4 2002.

5 Schoellhamer, D. H.: Sudden clearing of estuarine waters upon crossing the threshold from transport
6 to supply regulation of sediment transport as an erodible sediment pool is depleted: San Francisco
7 Bay, 1999, *Estuar. Coast.*, 34, 885–899, doi:10.1007/s12237-011-9382-x, 2011.

8 Schoellhamer, D. H., Wright, S. A., and Drexler, J.: A conceptual model of sedimentation in the
9 Sacramento–San Joaquin Delta, *San Francisco Estuar. Watershed Sci.*, 10, 2012.

10 Sutherland, T. F., Lane, P. M., Amos, C. L., and Downing, J.: The calibration of optical backscatter
11 sensors for suspended sediment of varying darkness levels, *Mar. Geol.*, 162, 587–597,
12 doi:10.1016/S0025-3227(99)00080-8, 2000.

13 Syvitski, J. P. M. and Kettner, A. J.: Sediment flux and the Anthropocene, *Philos. T. Roy. Soc. A*, 369,
14 957–975, doi:10.1098/rsta.2010.0329, 2011.

15 van der Wegen, M., Ja_e, B. E., and Roelvink, J. A.: Process-based, morphodynamic hindcast of
16 decadal deposition patterns in San Pablo Bay, California, 1856–1887, *J. Geophys. Res.- Earth*, 116,
17 F02008, doi:10.1029/2009jf001614, 2011.

18 van der Wegen, M., and Roelvink, J. A.: Reproduction of estuarine bathymetry by means of a
19 process-based model: Western Scheldt case study, the Netherlands, *Geomorphology*, 179,
20 152–167, 10.1016/j.geomorph.2012.08.007, 2012.

21
22 Vörösmarty, C. J., Meybeck, M., Fekete, B., Sharma, K., Green, P., and Syvitski, J. P. M.:
23 Anthropogenic sediment retention: major global impact from registered river impoundments, *Global*
24 *Planet. Change*, 39, 169–190, doi:10.1016/S0921-8181(03)00023-7, 2003.

25 Whipple, A., Grossinger, R., Rankin, D., Stanford, B., and Askevold, R.: Sacramento–San Joaquin
26 Delta historical ecology investigation: exploring patterns and process, San Francisco Estuary Institute
27 – Aquatic Science Center, Richmond, CA, 2012.

28 Whitcraft, C. R. and Levin, L. A.: Regulation of benthic algal and animal communities by salt marsh
29 plants: impact of shading, *Ecology*, 88, 904–917, doi:10.1890/05-2074, 2007.

30 Willmott, C. J.: ON THE VALIDATION OF MODELS, *Physical Geography*, 2, 184–194,
31 10.1080/02723646.1981.10642213, 1981.
32

- 1 Winterwerp, J. C., Manning, A. J., Martens, C., de Mulder, T., and Vanlede, J.: A heuristic
2 formula for turbulence-induced flocculation of cohesive sediment, *Estuarine, Coastal and*
3 *Shelf Science*, 68, 195-207, 10.1016/j.ecss.2006.02.003, 2006.
- 4
5 Wright, S. A. and Schoellhamer, D. H.: Trends in the sediment yield of the Sacramento River,
6 California, 1957–2001, *San Francisco Estuar. Watershed Sci.*, 2, 2004.
- 7 Wright, S. A. and Schoellhamer, D. H.: Estimating sediment budgets at the interface between rivers
8 and estuaries with application to the Sacramento–San Joaquin River Delta, *Water Resour. Res.*, 41,
9 W09428, doi:10.1029/2004wr003753, 2005.
- 10 Yahg, S. L.: The role of scirpus marsh in attenuation of hydrodynamics and retention of fine sediment
11 in the Yangtze estuary, *Estuar. Coast. Shelf S.*, 47, 227–233, 1998.
- 12

1 Table 1: Parameters set of sensitivity analysis.

2

Parameters		Minimum	Maximum
standard		$w = 0.25$; $\tau = 0.25$; $M = 1 \cdot 10^{-4}$	
Fall velocity	w_s (mm s ⁻¹)	0.15	0.38
Critical shear stress	τ_{cr} (Pa)	0.125	0.5
Erosion Coefficient	M (kg m ² s ⁻¹)	$2.5 \cdot 10^{-5}$	$1 \cdot 10^{-2}$

3

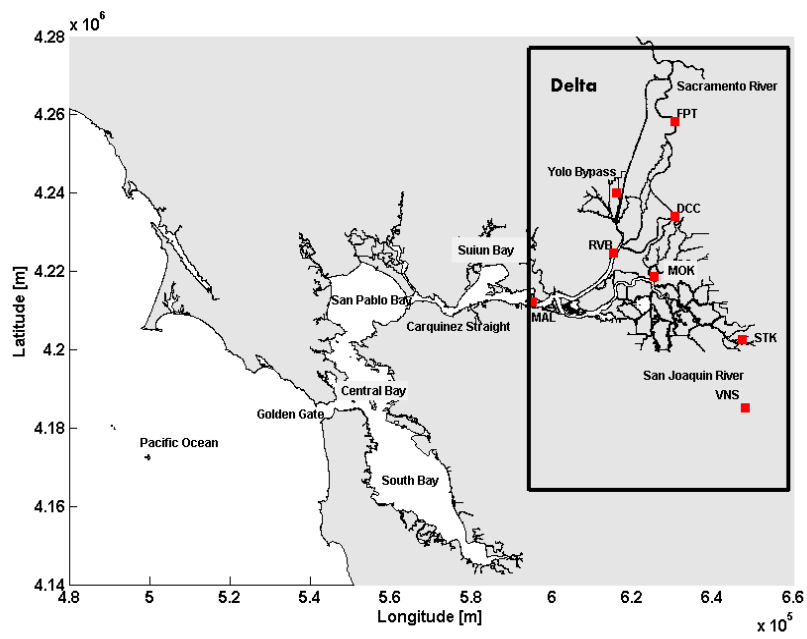


Fig 1: San Francisco Bay-Delta, the black rectangle highlights the Delta, and the red squares indicate measurement stations.

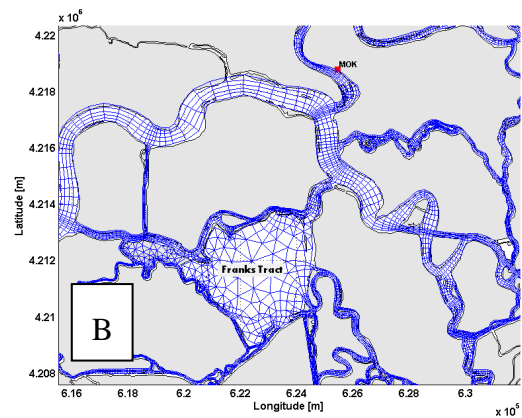
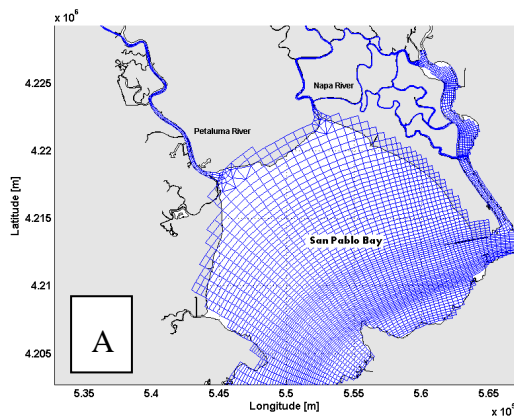
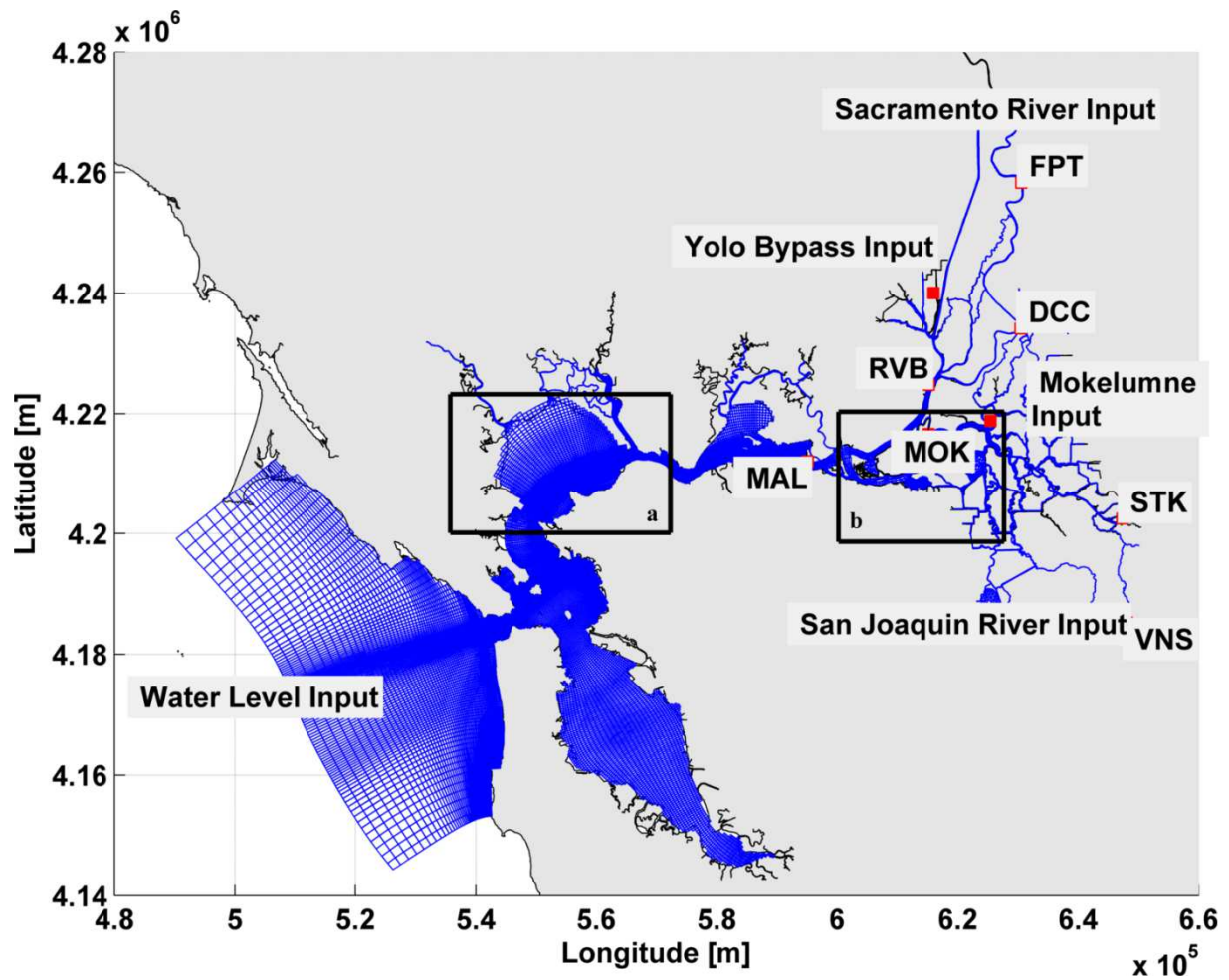


Fig 2: Numerical mesh, the red dots indicate the calibration stations. (<http://san-francisco-bay-delta-model.unesco-ihe.org/>). Zoom in the computational grid, A) San Pablo Bay connecting to Petaluma and Napa Rivers, B) Delta channels and Franks Tract.

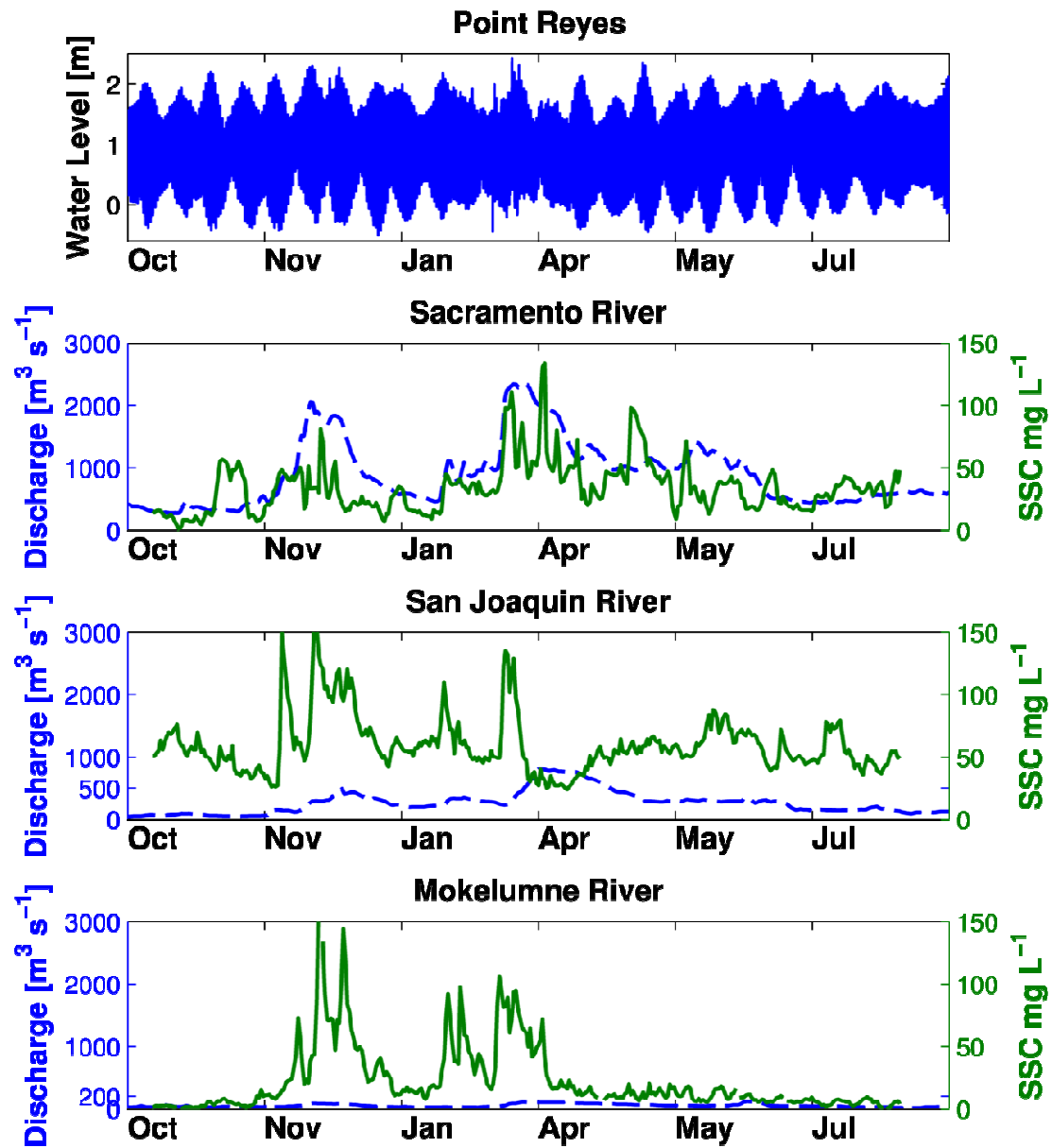


Fig 3: Input boundary condition. Top panel water level at Point Reyes, the following 3 panels show discharge in dashed blue line and SSC in solid green line for Sacramento River at FPT, San Joaquin River at VNS and Mokelumne River at Woodbridge respectively.

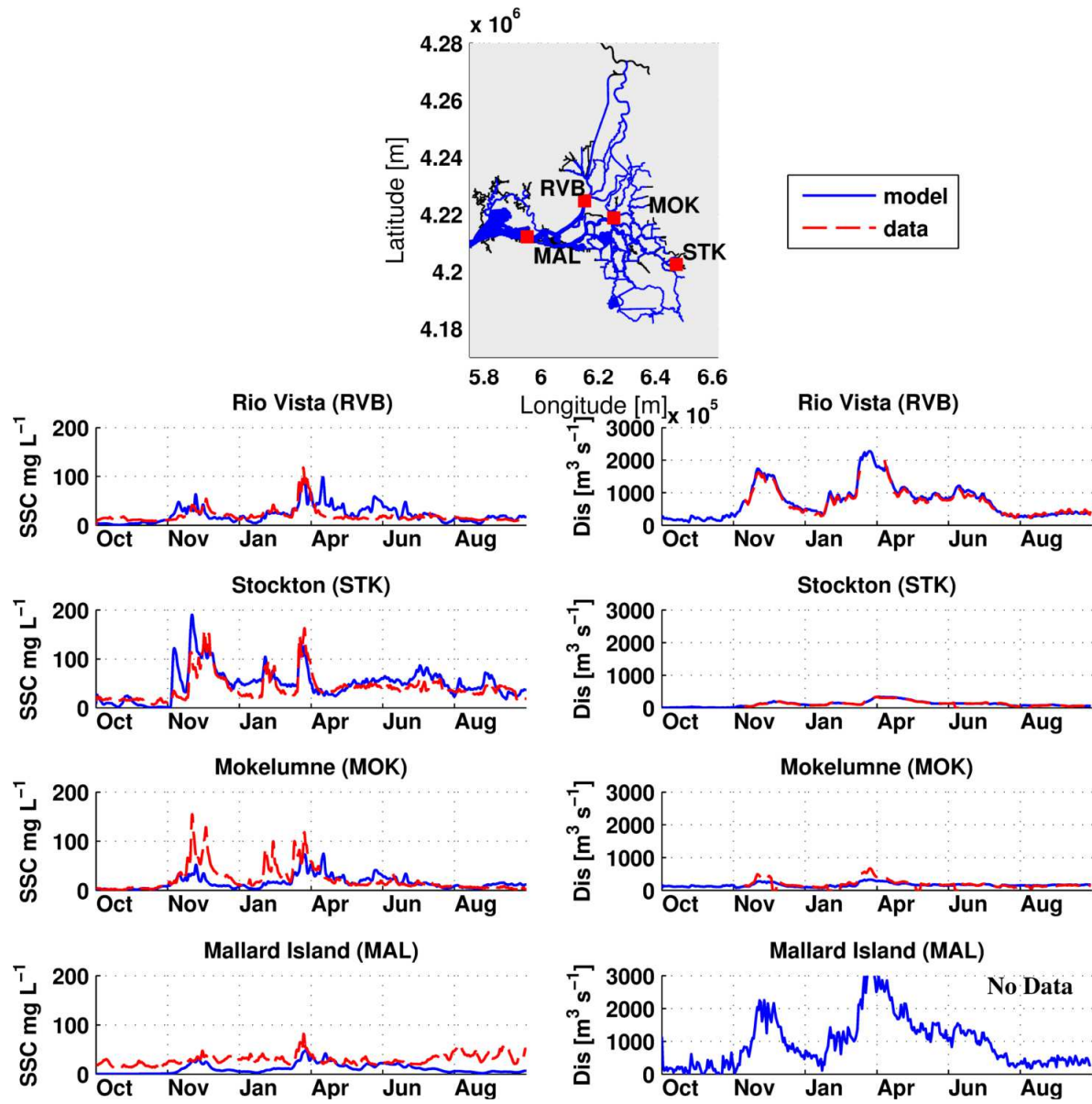
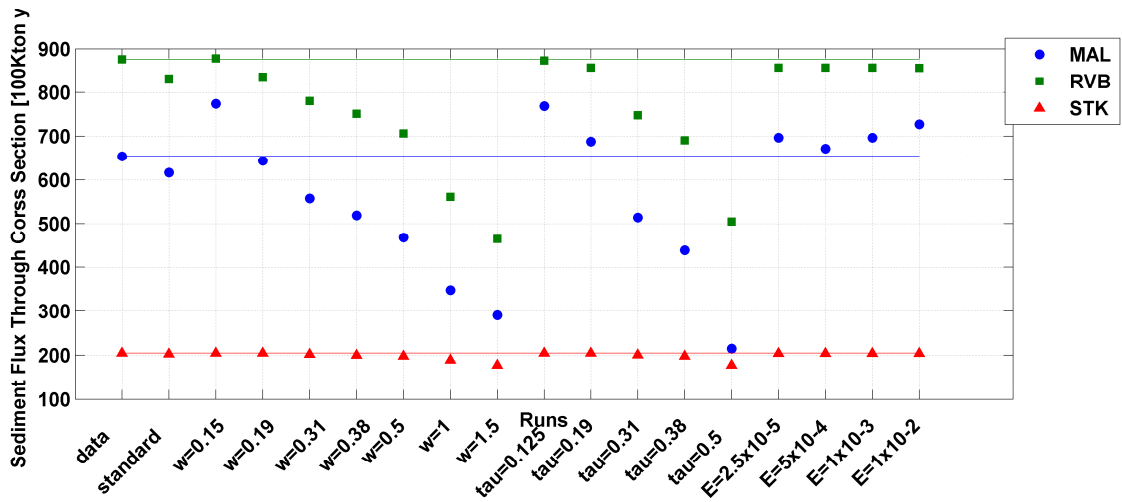


Fig 4: Calibration stations location top Fig. Left panels show SSC calibration and right panels show discharge. Data are dashed red lines and model results are solid blue lines. Note that in the discharge plots of RVB and STK the data line is behind the model line.

1
2



3

4 Fig 5: Sensitivity analysis of sediment flux, for 3 stations, RVB in green squares (Sacramento
5 River), STK in red triangles (San Joaquin River) and MAL in blue circles (Delta output). The
6 colour lines indicate the data values.

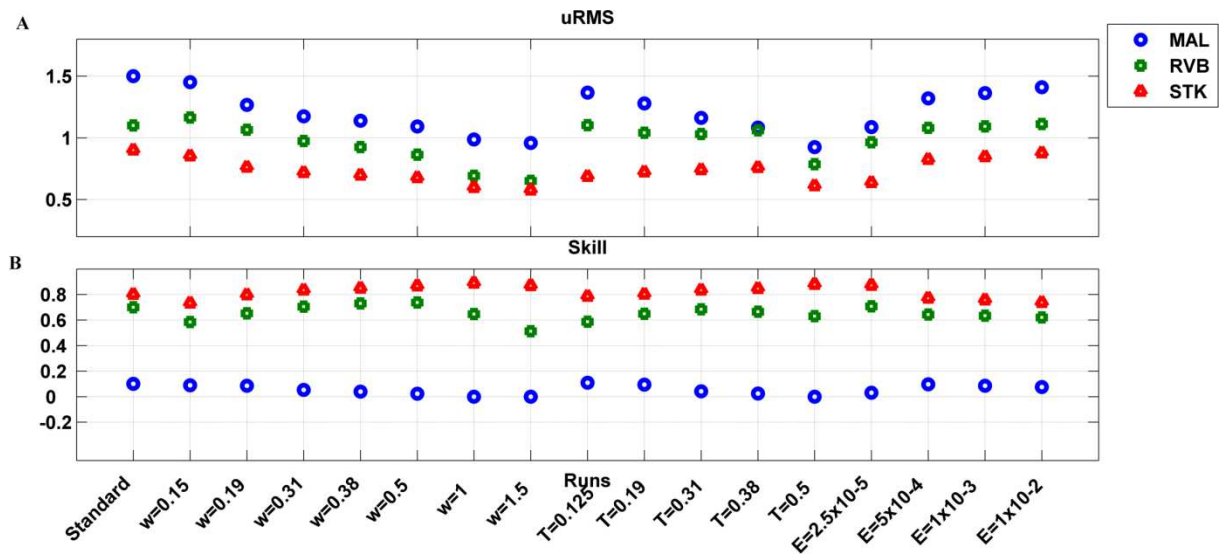


Fig 6: Statistical metrics in (a) Unbiased Root Mean Square and in (b) Skill. In the x axis are the different runs and the colors the stations RVB (green square), STK (red triangle) and MAL (blue circle).

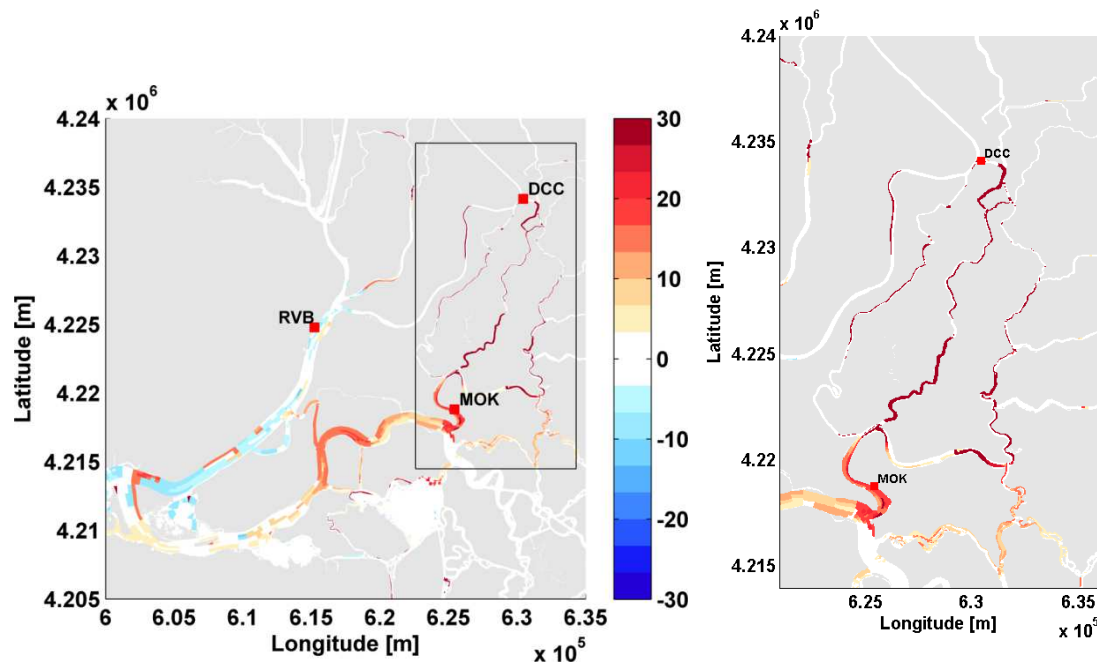
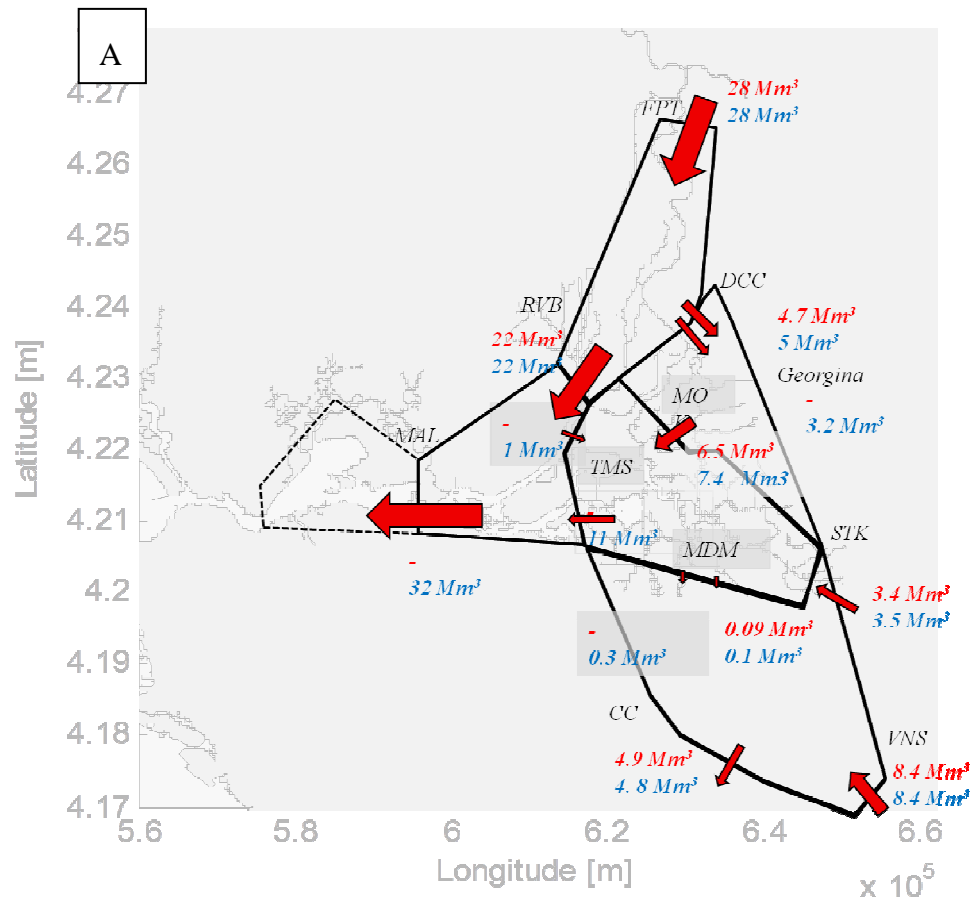


Fig 7: Anomaly of a SSC (mg L^{-1}) snapshot between a run with open and one with closed DCC, this pattern is representative in time as well. The right panel is a zoom in between the DCC and MOK (black rectangle). Red shades represent regions where the SSC level is higher in the open than the close scenario, the blue shades where it was lower.



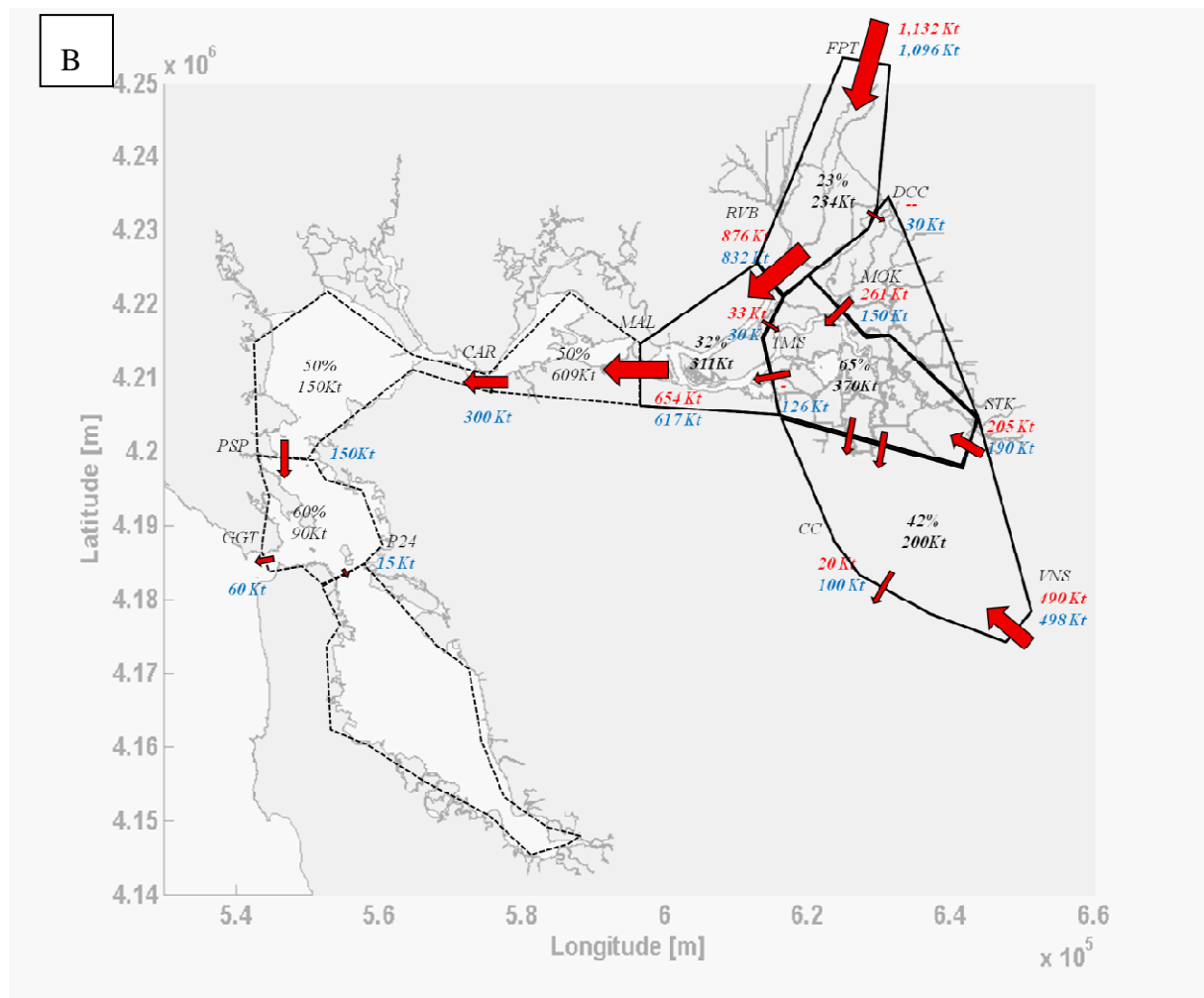


Fig 8: Water Discharge (A) and Sediment Flux (B) Path models. The arrows represent the water (A) and sediment (B) fluxes through the cross sections. Area of the arrow is proportional to the flux. Red/blue indicates the sediment (water) fluxes from data/model. Inside each polygon is the sediment budget for the area. The Bay portion is dashed because the model is 2D and 3D processes occur in that region.

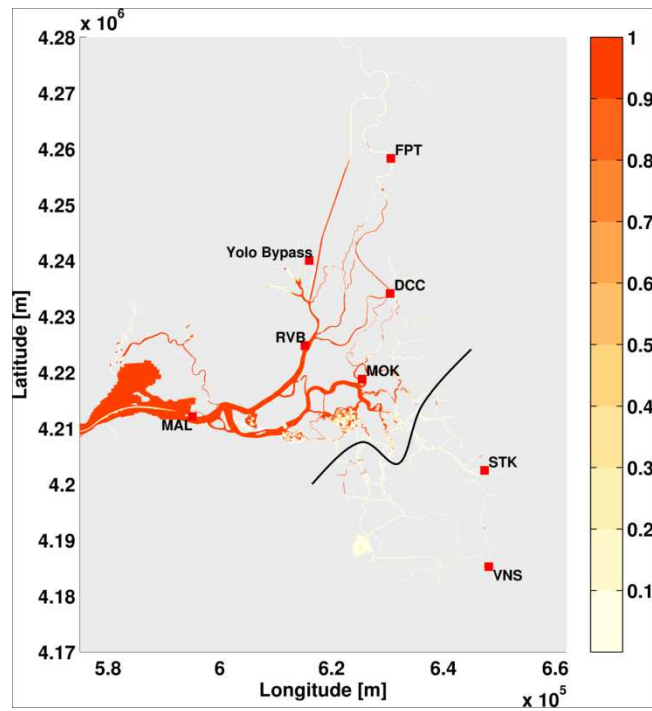


Fig 9: Sediment bottom composition after one year, starting with no bed sediment available. In Red shades region dominated by Sacramento and in white by San Joaquin, the black line highlights this separation.

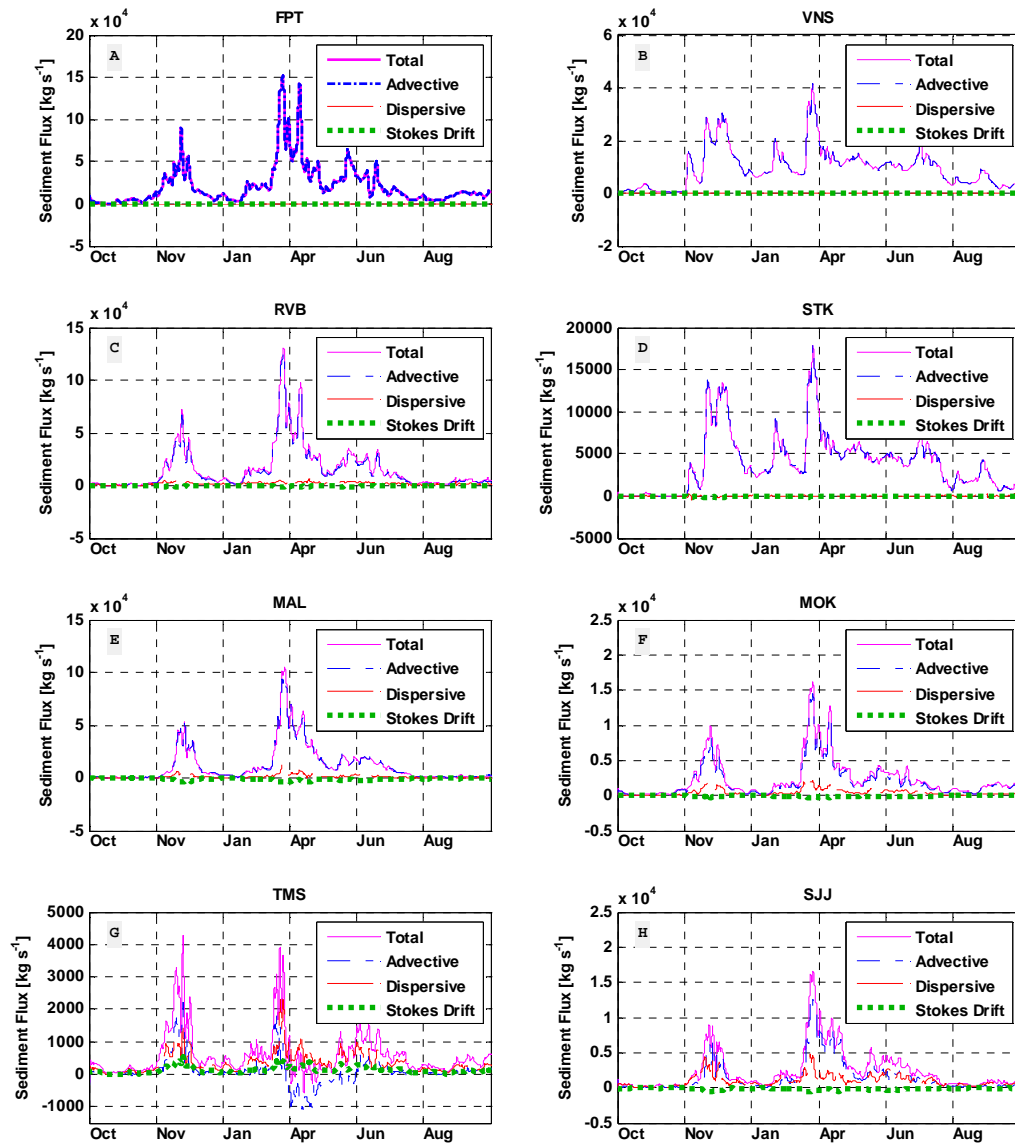
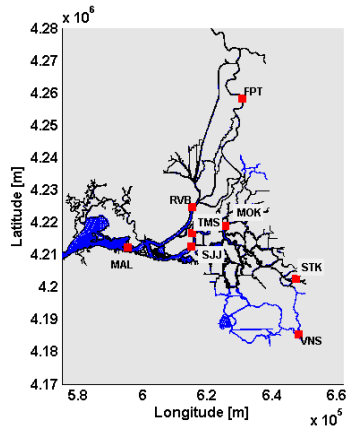


Fig 10: Flux calculation for several stations within the Delta. Figs A, C, E, and G show the flux change following Sacramento branch and B, C, F and H following San Joaquin branch. The total flux is represented in magenta (in FPT and VNS the total is the same as the

- 1 advective), in blue the advective flux, in red the dispersive flux and in green Stokes drift.
- 2 (Positive is seaward).
- 3

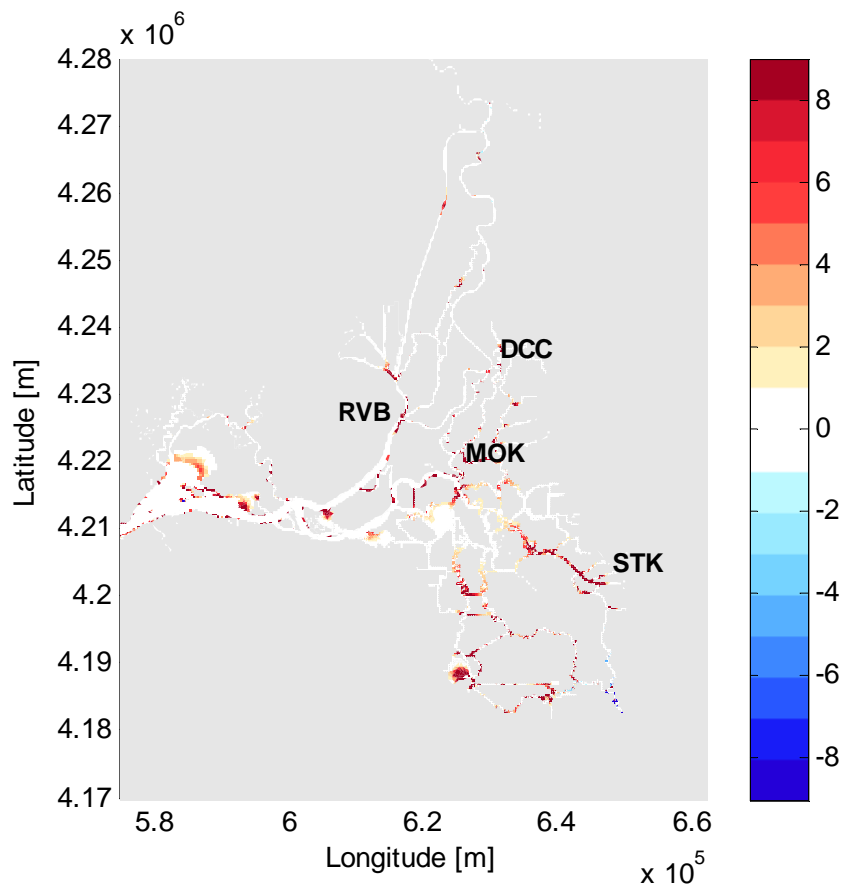


Fig 11: DELWAQ deposition volume translated in bottom sediment deposition in [mm].

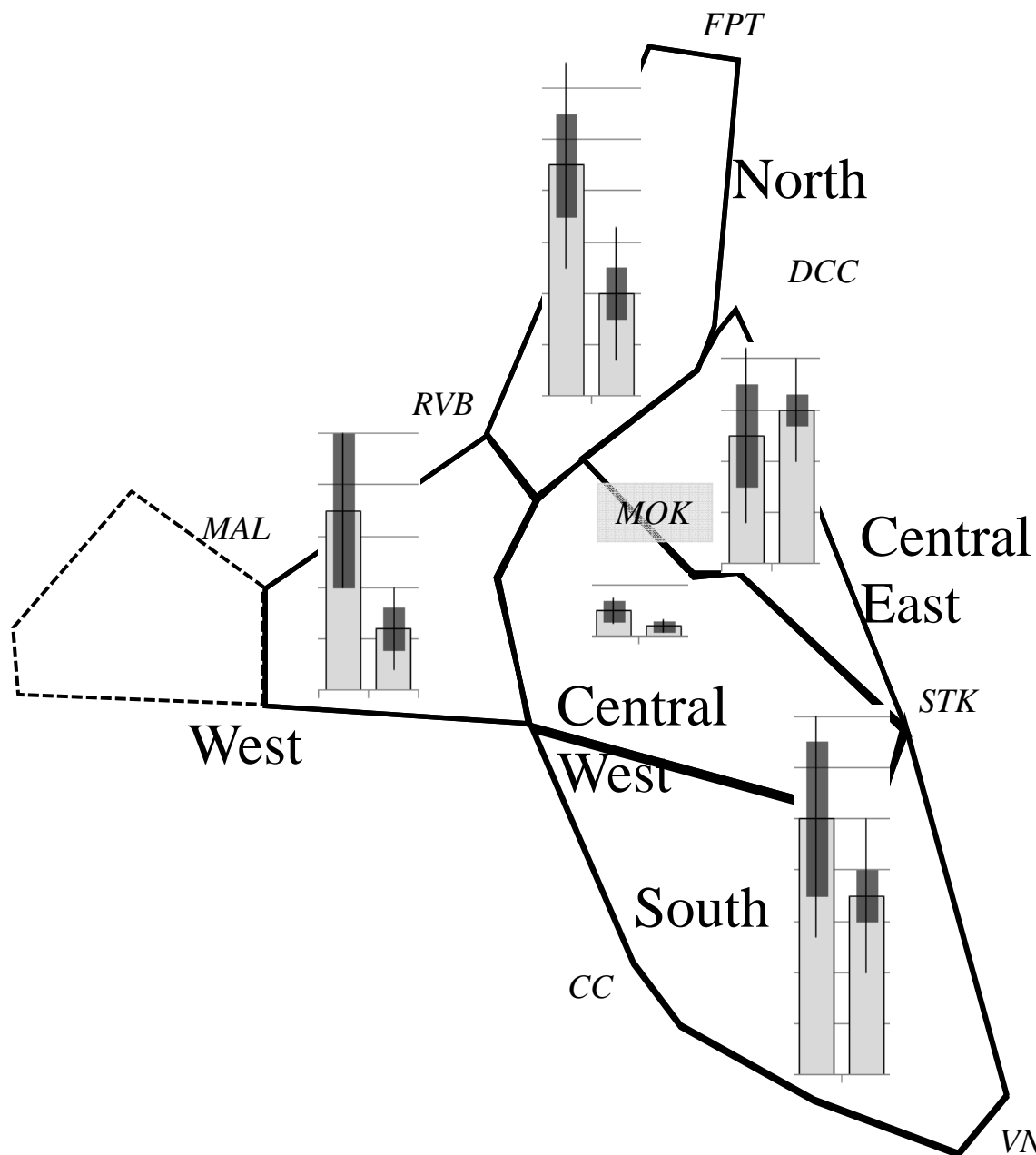


Fig 12: Turbidity histogram for each Delta area, the left hand side bars indicates wet season and the ones in the right dry season. The light gray bar indicate the mean turbidity over the area, the darker bar the spatial deviation and the lines the daily deviation. Each horizontal line represents 10 ntu.

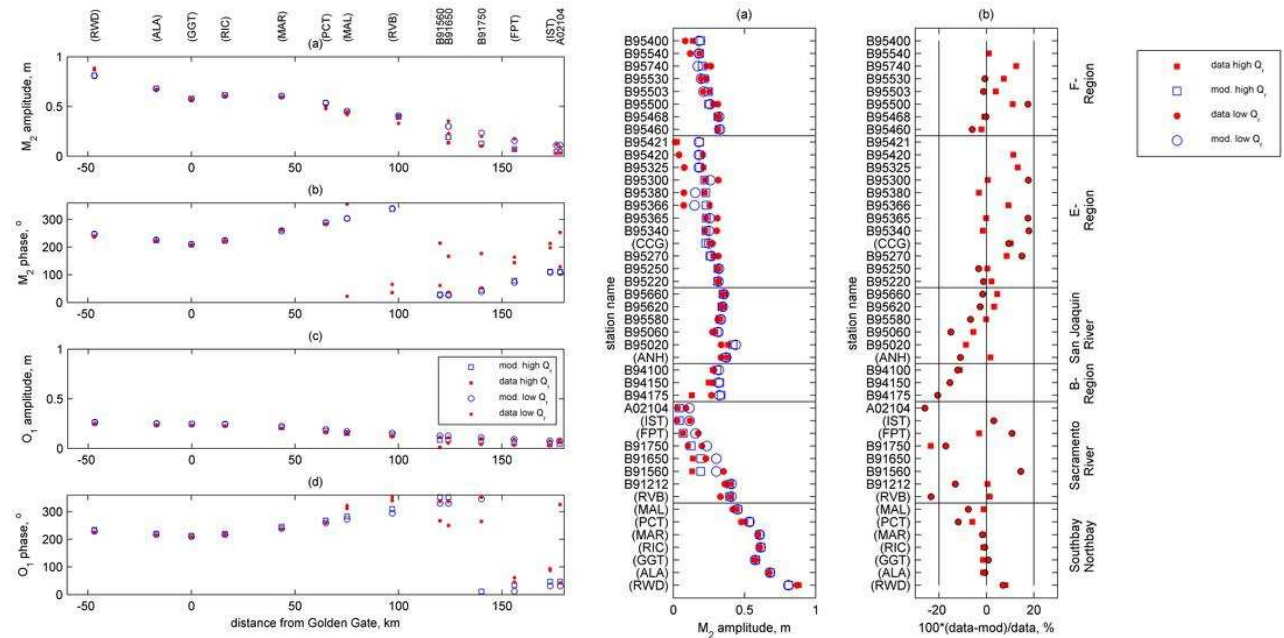
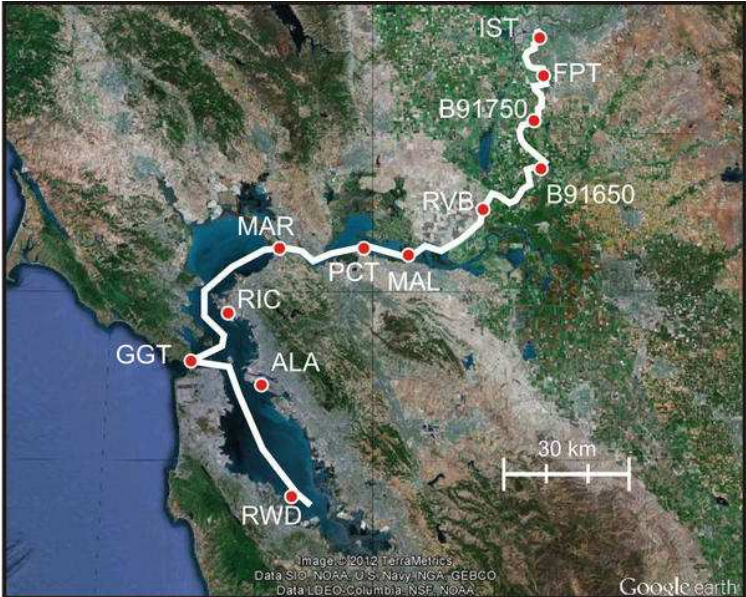


Fig A1: Hydrodynamic calibration example.

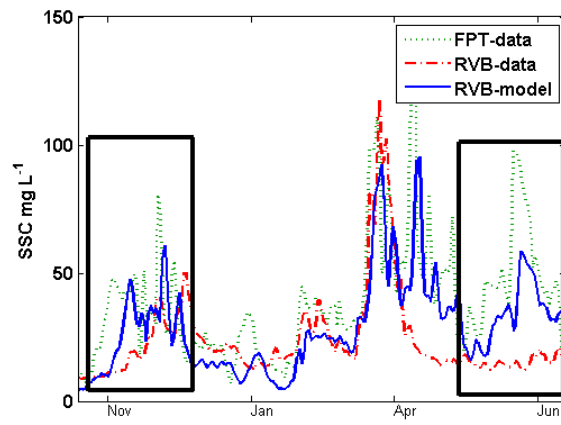
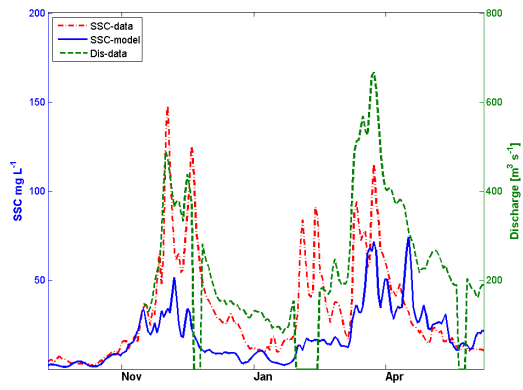


Fig B1: Comparison between SSC levels in RVB station in situ data (dashed red) and model result (solid blue) and FPT station (dotted green).



1

2 Fig B2: Water discharge (model) and SSC level (data and model) in MOK station.

3

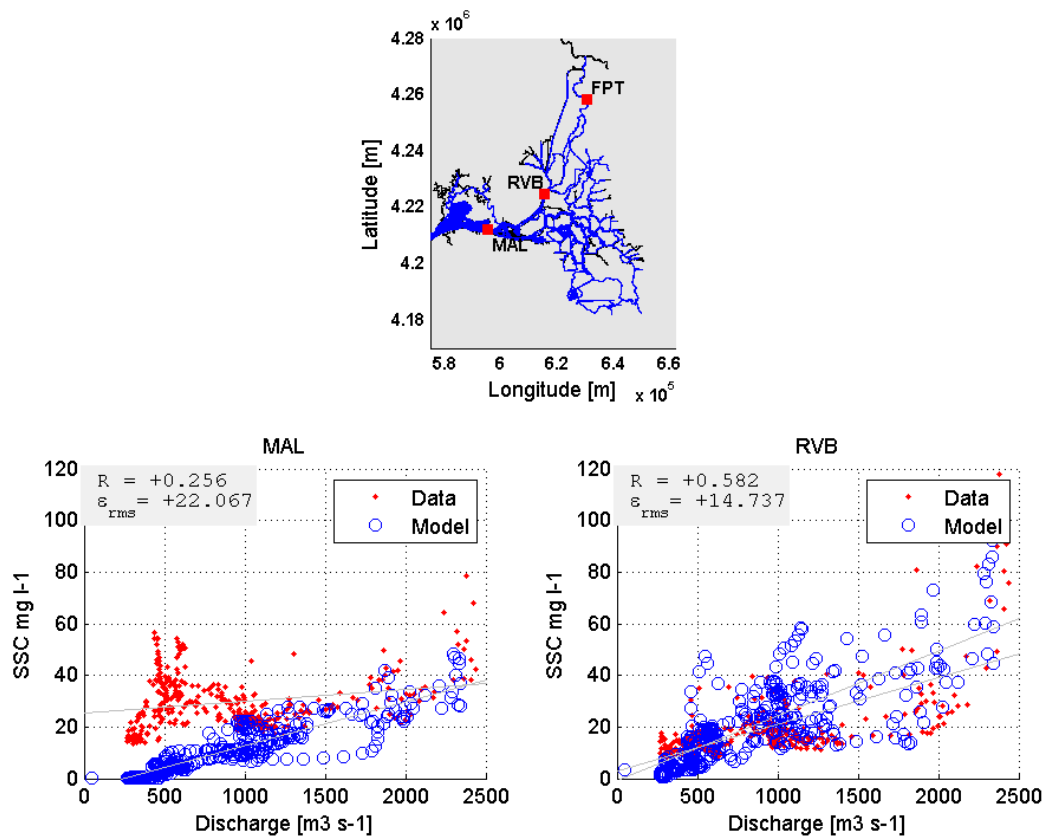


Fig B3: Scatter plot Discharge versus SSC. Showing on the left (MAL) for MAL station and on the right hand (RVB) side RVB station. The red dots represent the Data and the blue model results.